



Acidification, deoxygenation, and nutrient and biomass declines in a warming Mediterranean Sea

Marco Reale¹, Gianpiero Cossarini¹, Paolo Lazzari¹, Tomas Lovato², Giorgio Bolzon¹, Simona Masina², Cosimo Solidoro¹, and Stefano Salon¹

¹National Institute of Oceanography and Applied Geophysics – OGS, Trieste, Italy

²Ocean Modeling and Data Assimilation Division, Fondazione Centro Euro-Mediterraneo sui Cambiamenti Climatici, CMCC, Bologna, Italy

Correspondence: Marco Reale (mreale@ogs.it) and Stefano Salon (ssalon@ogs.it)

Received: 9 November 2021 – Discussion started: 20 November 2021

Revised: 27 May 2022 – Accepted: 16 June 2022 – Published: 1 September 2022

Abstract. The projected warming, nutrient decline, changes in net primary production, deoxygenation and acidification of the global ocean will affect marine ecosystems during the 21st century. Here, the climate change-related impacts on the marine ecosystems of the Mediterranean Sea in the middle and at the end of the 21st century are assessed using high-resolution projections of the physical and biogeochemical state of the basin under Representative Concentration Pathways (RCPs) 4.5 and 8.5. In both scenarios, the analysis shows changes in the dissolved nutrient contents of the euphotic and intermediate layers of the basin, net primary production, phytoplankton respiration and carbon stock (including phytoplankton, zooplankton, bacterial biomass and particulate organic matter). The projections also show uniform surface and subsurface reductions in the oxygen concentration driven by the warming of the water column and by the increase in ecosystem respiration as well as an acidification signal in the upper water column linked to the increase in the dissolved inorganic carbon content of the water column due to CO₂ absorption from the atmosphere and the increase in respiration. The projected changes are stronger in the RCP8.5 (worst-case) scenario and, in particular, in the eastern Mediterranean due to the limited influence of the exchanges in the Strait of Gibraltar in that part of the basin. On the other hand, analysis of the projections under the RCP4.5 emission scenario shows a tendency to recover the values observed at the beginning of the 21st century for several biogeochemical variables in the second half of the period. This result supports the idea – possibly based on the existence in a system such as the Mediterranean Sea of a certain buffer

capacity and renewal rate – that the implementation of policies for reducing CO₂ emission could indeed be effective and could contribute to the foundation of ocean sustainability science and policies.

1 Introduction

The Mediterranean Sea (Fig. 1) is a midlatitude semienclosed basin surrounded by the continental areas of Southern Europe, Northern Africa and the Middle East. The basin is characterized by a thermohaline circulation composed of three distinctive cells. The first is an open cell associated with the inflow of Atlantic Water (AW) at the Strait of Gibraltar (which undergoes a progressive increase in salinity due to evaporation, becoming Modified Atlantic Water, or MAW) and the formation of Levantine Intermediate Water (LIW) in the Eastern Basin (Lascaratos, 1993; Nittis and Lascaratos, 1998; Velaoras et al., 2019; Fach et al., 2021; Fedele et al., 2022). The other two are closed cells associated with deep water formation processes occurring in the Gulf of Lion (located in the north Western Mediterranean, Fig. 1; Somot et al., 2018 and reference therein) and in the Adriatic Sea (Fig. 1; Mantziafou and Lascaratos, 2004, 2008; Schroeder et al., 2012 and references therein).

Future climate projections for the Mediterranean region based on different emission scenarios show, at the end of the 21st century, (i) a reduction in precipitation and a general warming of the area (e.g., Giorgi, 2006; Diffenbaugh et al., 2007; Giorgi and Lionello, 2008; Dubois et al., 2012;

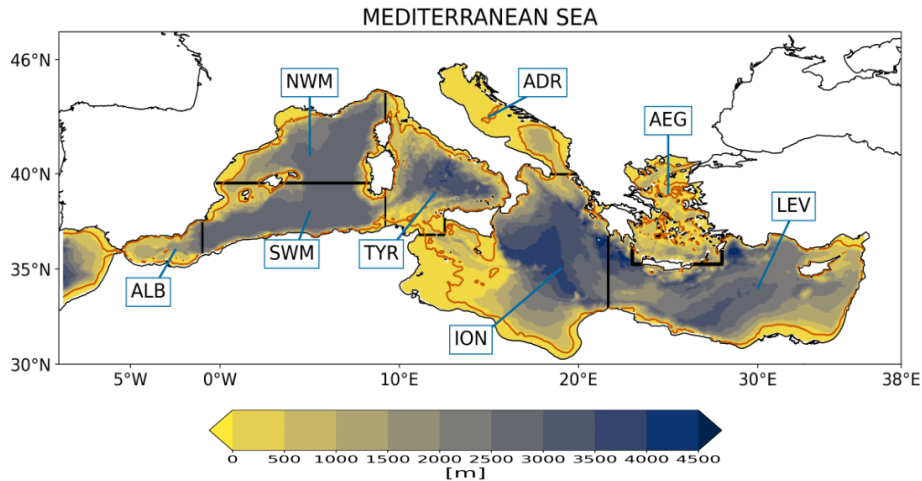


Figure 1. Mediterranean Sea bathymetry (in m) and relative sub-basins considered in the analysis: the Alboran Sea (ALB), North Western Mediterranean (NWM), South Western Mediterranean (SWM), Tyrrhenian (TYR), Adriatic Sea (ADR), Ionian Sea (ION), Aegean Sea (AEG) and Levantine Basin (LEV). The dark orange line marks the 200 m isobath in the model domain. The domain boundary is set at longitude 8.8° W, westward of the Strait of Gibraltar.

Lionello et al., 2012; Planton et al., 2012; Gualdi et al., 2013; MedEEC, 2020), (ii) a warming of seawater (Somot et al., 2006; Adloff et al., 2015; Soto-Navarro et al., 2020; MedECC, 2020), and (iii) a consistent weakening of the thermohaline circulation, an increase in the stratification index throughout the basin (Somot et al., 2006; Adloff et al., 2015; Soto-Navarro et al., 2020) and further increases in the frequency and severity of atmospheric and marine heatwaves and droughts (Galli et al., 2017; Darmaraki et al., 2019; Ibrahim et al., 2021; Mathbout et al., 2021). Conversely, the future evolution of sea surface salinity in the Mediterranean Sea and the sign of this change are still uncertain due to the role played by rivers and Strait of Gibraltar exchanges (Adloff et al., 2015; Soto-Navarro et al., 2020; MedECC, 2020). In general, the magnitude of the projected changes has been shown to be dependent on the adopted emission scenario (MedECC, 2020).

From a biogeochemical point of view, the Mediterranean Sea is considered an oligotrophic (ultraoligotrophic in its eastern part) basin (Bethoux et al., 1998; Moutin and Raimbault, 2002; Siokou-Frangou et al., 2010; Lazzari et al., 2012). It is characterized by low productivity levels and an east–west trophic gradient (Crise et al., 1999; D’Ortenzio and d’Alcala, 2009; Lazzari et al., 2012) which results from the superposition of different mechanisms such as the biological pump, the estuarine inverse circulation, and the positions of nitrate (NO_3) and phosphate (PO_4) sources (Crise et al., 1999; Crispi et al., 2001). The only exceptions to the oligotrophy of the basin are some areas (the Gulf of Lion, Strait of Sicily, Algerian coastlines, southern Adriatic Sea, Ionian Sea, Aegean Sea and Rhodes Gyre) where strong vertical mixing and upwelling phenomena associated with air–sea interactions and wind stress forcing enrich the surface in nutri-

ents, thus favoring rapid phytoplankton growth (or blooms), mostly in the late winter to early spring period (D’Ortenzio and Ribera d’Alcala, 2009; Reale et al., 2020b). A proxy that is widely adopted to detect phytoplankton blooms is the surface concentration of chlorophyll *a* (Chl-*a*), which is characterized by relatively high values in specific open-sea and coastal areas, where it is linked to the physical forcing and river inflow (D’Ortenzio and Ribera d’Alcala, 2009; Lazzari et al., 2012; Herrmann et al., 2013; Auger et al., 2014; Richon et al., 2018; Di Biagio et al., 2019; Reale et al., 2020a). The open-sea Chl-*a* vertical dynamics follow a seasonal cycle, with winter to early spring surface blooms and a summer onset of a deep Chl-*a* maximum (DCM), which deepens from approximately 50 m in the western areas to 100 m in the eastern areas (e.g., Lazzari et al., 2012; Macias et al., 2014; Lavigne et al., 2015; Cossarini et al., 2021).

Due to the strong links between ocean–atmosphere dynamics and biogeochemical patterns, it has to be expected that future climate changes will have relevant impacts on the biogeochemistry and, in turn, on the marine ecosystem dynamics of the Mediterranean Sea. In fact, all the projected changes for the region will likely affect the vertical mixing and reduce the nutrient supply into the euphotic layer of the Mediterranean Sea (e.g., Richon et al., 2019), which is essential for phytoplankton dynamics and productivity, with possible impacts on the biogeochemical carbon cycle and carbon dioxide (CO_2) exchange with the atmosphere (e.g., Lazzari et al., 2012; Cossarini et al., 2015; Canu et al., 2015; Solidoro et al., 2022).

An assessment of the effects of climate change on the biogeochemistry and marine ecosystem dynamics of the Mediterranean Sea has been considered in a number of previous studies based on different emission scenarios. Hermann

et al. (2014) assessed the response of the pelagic planktonic ecosystem of the North Western Mediterranean to different emission scenarios and showed that, at end of the 21st century, the biogeochemical processes and marine ecosystem components should be very similar to those observed at the end of the 20th century, although quantitative differences might be observed, such as increases in bacterial growth, gross primary production and the biomass of the small-size phytoplankton group. Lazzari et al. (2014) found a negative change in the plankton biomass in response to the A1B emission scenario, resulting from an increase in productivity and community respiration. Benedetti et al. (2018), using environmental niche models and considering six physical simulations based on different emission scenarios (A2, A2-F, A2-RF, A2-ARF, A1B-ARF, B1-ARF; Adloff et al., 2015), projected, in response to climate change, a loss of copepod diversity throughout most of the surface layer of the Mediterranean Sea. On the other hand, Moullec et al. (2019) found an increase and decrease in both phytoplankton biomass and net primary production by the end of the 21st century in the eastern and western Mediterranean Sea under the RCP8.5 emission scenario. Macias et al. (2015) showed that, under emission scenarios RCP4.5 and RCP8.5, and despite a significant observed warming trend, the mean integrated primary production rate in the entire basin will remain almost unchanged in the 21st century. However, they pointed out some peculiar spatial differences in the basin, such as an increase in the oligotrophy of the Western Basin due to a surface density decrease and an increase in net primary production in the Eastern Basin due to the increased density. Richon et al. (2019) observed, under the A2 emission scenario (which is similar to the RCP8.5 emission scenario in terms of the magnitude of the projected changes in global mean temperature), an accumulation of nitrate in the basin and a reduction of 10 % in net primary productivity by 2090, with a peak of 50 % in specific areas (including the Aegean Sea). On the other hand, no tendencies for phosphorus were observed. Pagès et al. (2020) showed, under emission scenario RCP8.5, a decline in the nutrient concentration (stronger in NO_3 than in PO_4) at the surface of the basin due to the increase in vertical stratification, and pointed out that the Mediterranean Sea will become less productive (a 14 % decrease in integrated primary production in both the Western and Eastern basins) and will be characterized by a reduction (22 % in the Western Basin and 38 % in the Eastern Basin) in large phytoplankton species abundance in favor of small organisms. All these changes will mainly affect the Western Basin, while the Eastern Basin will be less impacted (Pagès et al., 2020). Solidoro et al. (2022) discussed the evolution of the carbon cycling, budgets and fluxes of the basin under the A2 scenario, highlighting an increase in the trophodynamic carbon fluxes and showing, at the same time, that the increment in the plankton primary production will be more than compensated for by the increase in the ecosystem total respiration, which corresponds to a decrease in the total living carbon and oxy-

gen in the epipelagic layer. Moreover, Solidoro et al. (2022) also projected an increase in the dissolved inorganic carbon (DIC) pool and quantified, for the first time, the related acidification of the basin – a process that might significantly alter Mediterranean ecosystems (Zunino et al., 2017, 2019) and their capability to sustain ecosystem services (Zunino et al., 2021).

All of the abovementioned works demonstrate that the dynamics of the marine ecosystem may be affected directly and indirectly by climate change, and the magnitude of their response is dependent on the emission scenario adopted. Different levels of warming, acidification and changes in the vertical distributions of the oxygen, nutrient concentration and net primary production related to water column stratification are all potential marine stressors affecting marine organisms and ecosystem dynamics (see Kwiatkowski et al., 2020 for a review of the synergistic effects among potential marine stressors).

A proper simulation of these marine stressors and related impacts requires the adoption of suitable horizontal and vertical resolutions. In fact, it has been shown that meso- and submesoscale structures of the Mediterranean circulation do indeed influence the biogeochemical dynamics of many areas of the basin (Moutin and Prieur, 2012; Richon et al., 2019), while the vertical resolution affects the features of the simulated stratification and subsurface ventilation pathways (see Kwiatkowski et al., 2020 and references therein for a review).

These considerations emphasize the importance of providing eddy-resolving future projections of the Mediterranean Sea biogeochemistry under different emission scenarios. In fact, although observational and modeling studies have been already carried out in the recent period to assess the importance of the mesoscale dynamics for the physical and biogeochemical states of limited areas of the Mediterranean Sea (e.g., Hermann et al., 2008; Moutin and Prieur, 2012; Guyennon et al., 2015; Ramirez-Romero et al., 2020), long-term eddy-resolving biogeochemical projections under different emission scenarios have not yet, to the best of the authors' knowledge, been analyzed for this region. Such projections might be used in future studies specifically focused on the analysis of climate change impacts on specific organisms, habitats and/or local areas.

Therefore, climate change-related impacts on the marine ecosystems of the Mediterranean Sea in the middle and at the end of the 21st century are assessed here using eddy-resolving projections of the physical and biogeochemical state of the basin under emission scenarios RCP4.5 and RCP8.5. These projections are derived from the offline coupling between the physical model MFS16 (Mediterranean Forecasting System at $1/16^\circ$; Oddo et al., 2009) and the transport-reaction model OGSTM-BFM (OGS Transport Model-Biogeochemical Flux Model; Lazzari et al., 2012). The analysis focuses on 21st century projected changes in dissolved nutrients and oxygen, net primary production, phytoplankton respiration, living and nonliving organic matter,

plankton and bacterial carbon biomass, and particulate organic matter (POC). Moreover, the response of the basin to the increasing atmospheric CO₂ concentration is thoroughly investigated. The projected changes are also correlated with changes in the physical forcing in the region.

The article is organized as follows: the MFS16-OGSTM-BFM model system and the climate scenario setups are described in Sect. 2. Section 3 discusses the projected impacts on the marine ecosystems of the Mediterranean basin. Finally, Sect. 4 summarizes and discusses the results of this work, together with their uncertainties, paving the way for possible future research avenues.

2 Data and methods

The biogeochemical projections of the Mediterranean Sea state during the 21st century are produced by driving the transport-reaction model OGSTM-BFM (Lazzari et al., 2012) with the 3D outputs of the physical model MFS16 (Oddo et al., 2009) through offline coupling. In fact, the physical model MFS16 supplies the OGSTM-BFM with the temporal evolution of the daily horizontal and vertical current velocities, vertical eddy diffusivity, potential temperature, salinity, and surface data for solar shortwave irradiance and wind stress. The resulting transport processes affecting the concentrations of biogeochemical tracers (advection, vertical diffusion and sinking) are computed by OGSTM, which is a modified version of the OPA tracer model (Océan PARallélisé, Foujols et al., 2000). The temporal evolution of biogeochemical processes is computed by the Biogeochemical Flux Model (BFM; Vichi et al., 2015).

2.1 The MFS16 physical model

MFS16 is the Mediterranean configuration of the NEMO modeling system (Nucleus for European Modelling of the Ocean; Madec, 2008; see also <http://www.nemo-ocean.eu> (last access: 31 March 2022), version 3.4) and constitutes the climate implementation of the Mediterranean Ocean Forecasting System (Oddo et al., 2009; Lovato et al., 2013).

The original MFS16 domain covers the whole Mediterranean Sea and part of the neighboring Atlantic Ocean region with a horizontal grid resolution of $1/16^\circ$ (~ 6.5 km) and 72 unevenly spaced vertical levels (ranging from 3 m at the surface down to 600 m in the deeper layers; see Lovato et al., 2013). The model computes the air–sea fluxes of water, momentum and heat using specific bulk formulae tuned for the Mediterranean Sea (Oddo et al., 2009) and applied to the atmospheric fields obtained from the atmosphere–ocean general circulation model CMCC-CM (CMCC-Coupled Model; Scoccimarro et al., 2011).

The open boundary conditions in the Atlantic region for the physical variables (zonal/meridional components of the current velocity, sea surface height, temperature and salinity) were derived from the ocean component of the CMCC-CM coupled model, while the riverine freshwater discharges and fluxes in the Dardanelles Strait were provided by the hydrological component of the same coupled model (Gualdi et al., 2013). The initial conditions of the Mediterranean Sea were obtained from the gridded temperature and salinity data produced by the SeaDataNet infrastructure (<http://www.seadatanet.org/>, last access: 31 October 2020). The model was initially spun up for 25 years under the present climate conditions, and then scenario simulations were performed for the 2005–2100 period.

2.2 The OGSTM-BFM transport-reaction model

The OGSTM-BFM transport-reaction model is based on the coupling of a transport model (OGSTM) based on the OPA system (Foujols et al., 2000) with the BFM biogeochemical reactor. OGSTM-BFM is fully described in Lazzari et al. (2012, 2016), where it was used to simulate the Chl-*a*, primary production and nutrient dynamics of the Mediterranean Sea for the 1998–2004 period.

The OGSTM transport model resolves the advection, vertical diffusion and sinking terms of the biogeochemical tracers. The temporal scheme of OGSTM is an explicit forward temporal scheme for the advection and horizontal diffusion terms, whereas an implicit time scheme is adopted for the vertical diffusion. The BFM biogeochemical reactor considers co-occurring effects of multnutrient interactions and energy and material fluxes through the classical food chain and the microbial food web, which are both very important in the Mediterranean Sea (Bethoux et al., 1998). BFM has been extensively applied in studies of the dynamics of dissolved nutrients, Chl-*a* and net primary production in the Mediterranean Sea (Lazzari et al., 2012, 2016; Di Biagio et al., 2019; Reale et al., 2020a), marine carbon sequestration and alkalinity (Canu et al., 2015; Cossarini et al., 2015; Butenschön et al., 2021), impacts of climate change on the biogeochemical dynamics of marine ecosystems (Lazzari et al., 2014; Lamon et al., 2014; Solidoro et al., 2022), the influence of large-scale atmospheric circulation patterns on nutrient dynamics (Reale et al., 2020b), and operational short-term forecasts of the Mediterranean Sea biogeochemistry (Teruzzi et al., 2018, 2019; Salon et al., 2019). The version adopted here is v5.

The model simulates the biogeochemical cycles of carbon, nitrogen, phosphorus and silicon through dissolved forms and living organic and nonliving organic compartments (labile, semilabile and semirefractory organic matter). Moreover, it presently includes nine plankton functional types (PFTs) that are meant to be representative of diatoms, flagellates, picophytoplankton, dinoflagellates, carnivorous and omnivorous mesozooplankton, bacteria, heterotrophic nanoflagellates and microzooplankton. It also simulates the

carbonate system dynamics by solving the set of physico-chemical equilibria related to total alkalinity (ALK) and dissolved inorganic carbon (DIC) chemical reactions (Cossarini et al., 2015). ALK variability is driven by processes that alter the ion concentration in seawater (nitrification, denitrification, the uptake and release of nitrate, ammonia and phosphate by plankton cells, and the precipitation and dissolution of calcium carbonate, CaCO_3 ; see Wolf-Gladrow et al., 2007). The DIC dynamics are driven by biological processes (photosynthesis and respiration, precipitation and dissolution of CaCO_3) and physical processes (CO_2 exchange at the air-sea interface and, just as for all the other biogeochemical tracers, dilution–concentration due to evaporation minus precipitation processes).

2.3 Initial and boundary conditions for the biogeochemistry

Boundary conditions are adopted to represent the external supply of biogeochemical tracers and properties from the Strait of Gibraltar and the rivers into the Mediterranean Basin. The exchanges of nutrients and other biogeochemical tracers through the Strait of Gibraltar are achieved by relaxing the 3D fields in the Atlantic zone (Fig. 1) to average vertical profiles which, for dissolved oxygen, phosphate, nitrate and silicate, derive from Salon et al. (2019), while ALK is based on what was described in Cossarini et al. (2015). These profiles do not consider the seasonal cycle or the future temporal evolution, with DIC as the only exception, which is prescribed from a global ocean-climate simulation under the RCP8.5 emission scenario performed within the framework of the CMIP5 project (Coupled Model Inter-comparison Project Phase 5; Taylor et al., 2012) and based on the CMCC-CESM modeling system (CMCC-Coupled Earth System Model; Vichi et al., 2011). The reasons for these choices include (i) anomalous values observed for the N : P ratio in the RCP8.5 emission scenario, (ii) negligible variation, under emission scenario RCP8.5, of ALK during the 21st century, (iii) the lack of a consistent RCP4.5 scenario, and (iv) the possibility, using the same conditions at the Atlantic boundary, of testing the impacts of the different atmospheric and ocean forcings. Riverine inputs of phosphate, nitrate, dissolved oxygen, ALK and DIC are based on the PERSEUS FP7-287600 project dataset (Policy-oriented marine Environmental Research in the Southern European Seas; Van Apeldoorn and Bouwman, 2014) and do not include temporal evolution in the future scenarios in this case.

As observed in previous works (e.g., Richon et al., 2019), a transient scenario for the evolution of the atmospheric deposition of nitrogen and phosphorus over the Mediterranean Sea is presently not available. Following Di Biagio et al. (2019) and Reale et al. (2020a), the atmospheric deposition of phosphate and nitrate is parametrized as a mass flux at the surface and is set, for the entire basin, equal to $4780 \text{ Mmol yr}^{-1}$ for phosphate and $81275 \text{ Mmol yr}^{-1}$ for ni-

trate. Additional boundary conditions consider the sequestration of inorganic compounds in the marine sediment at the seabed.

The Representative Concentration Pathway (RCP) 4.5 and 8.5 emission scenarios (Moss et al., 2010) were used to force the coupled physical–biogeochemical MFS16-OGSTM-BFM system. RCP4.5 represents an intermediate scenario in which CO_2 emissions peak around 2040 (causing the maximum increase in CO_2 concentration) and then decline (with a resulting CO_2 concentration plateau), while RCP8.5 represents the worst-case scenario, in which CO_2 emissions (eventually driven by feedback effects such as the release of greenhouse gases from the permafrost) will continue to increase throughout the 21st century, and the $p\text{CO}_2$ concentration will rise to more than 1200 ppm by the end of the 21st century (IPCC, 2014). Recently, some authors have begun to consider the RCP8.5 scenario as “implausible,” being based, for example, on the use of coal at levels larger than its effective availability at the end of the 21st century (e.g., Hausfather and Peters, 2020). On the other hand, it is still widely used to assess the potential risks to the Mediterranean region (including marine ecosystems) that emerge in an extreme warm world climate ($+5^\circ\text{C}$) with respect to the preindustrial era (IPCC, 2014). Because of this, the projections obtained under this emission scenario are still discussed here.

The initial conditions for the dissolved oxygen, nutrient, silicate and carbonate system variables are based on the MEDAR-MEDATLAS dataset (Mediterranean Data Archeology and Rescue–Mediterranean Atlas), as described in Cossarini et al. (2015) and Salon et al. (2019).

Finally, all the simulations discussed in the next sections use as initial conditions the final fields resulting from a run that started on 1 January 2005 following a spin up of 100 years made with a loop over the 2005–2014 period for the physical forcing, the river nutrient discharge and the atmospheric forcing (nutrient deposition and CO_2 air value).

2.4 Simulation protocol and setup

Long-term simulations can be affected by drifts in state variables due to the imbalance among boundary conditions, transport processes and internal element cycle formulations of the biogeochemical model. Therefore, a specific simulation protocol based on the use of a control/scenario pair of simulations is implemented in order to disentangle the climate change signal from spurious signals (Solidoro et al., 2022). The protocol consists of a control simulation (CTRL) of 95 years and two 95-year biogeochemical scenario simulations, RCP4.5 and RCP8.5 (Fig. S1 in the Supplement). All the simulations adopt the final fields resulting from the spin-up simulation as initial conditions (Sect. 2.3). The CTRL is performed by repeating the 2005–2014 physical forcing and river discharge over the remaining 2015–2100 period (Fig. S1 in the Supplement). The difference between each

biogeochemical scenario and the CTRL provides the future evolution of the biogeochemical variable due to climate forcing.

Under each specific emission scenario and in the CTRL, our simulation protocol computes the time series of the mean annual 3D fields of the following variables: dissolved nutrients and oxygen, Chl-*a*, net primary production, phytoplankton respiration, organic matter, plankton and bacterial carbon biomass, POC, DIC, and pH.

First, the annual 3D fields are vertically averaged over two separate key vertical levels: the surface zone and the intermediate zone. The first one spans the upper 100 m of the water column, which represents the location of MAW and the euphotic layer of the basin, where most biological activities are concentrated. The second one covers the 200–600 m level, which includes the location of LIW. For the net primary production and phytoplankton respiration only, the vertical integral over the 0–200 m layer is considered (Lazzari et al., 2012).

Second, the temporal evolution of the unbiased scenario starting from the present state, $U(k)_{\text{SCEN}}$ (with $k = 2005, \dots, 2099$), is defined as

$$U(k)_{\text{SCEN}} = X'_{\text{SCEN}} + X(k)_{\text{SCEN}} - X(k)_{\text{CTRL}}, \quad (1)$$

where X'_{SCEN} is the average of $X(k)_{\text{SCEN}}$ over the 2005–2020 period (hereafter the PRESENT, Fig. S1), and $X(k)_{\text{SCEN}}$ and $X(k)_{\text{CTRL}}$ are the yearly averages in the scenario and CTRL simulations, respectively. We introduce the concept of an “unbiased scenario” because Eq. (1) removes the effect of potential model drifts due to unbalanced boundary conditions and model errors. The time series of CTRL are filtered with a linear regression to keep the long-term drift and remove spurious variability. The period 2005–2020 is chosen as a reference (as it is in the forthcoming validation too) due to the availability, after the year 2000, of more advanced satellite and assimilated datasets to evaluate the biogeochemistry of the basin and because it avoids any overlap between the historical and scenario parts of the simulations (with the former ending in 2004 and the latter starting in 2005). It is important to stress here that the choice of the period should not significantly affect the results of the study, as the observed differences during this period between the two scenarios for temperature, salinity and current speed fields have been found to be statistically nonsignificant over most of the basin (not shown).

Finally, the temporal evolution of the climate change signal (CCS) with respect to the present is given by

$$\text{CCS}(k)_{\text{SCEN}} = U(k)_{\text{SCEN}} - U_{\text{SCEN-PRESENT}}, \quad (2)$$

where $U_{\text{SCEN-PRESENT}}$ is the average of $U(k)_{\text{SCEN}}$ in the PRESENT. Hereafter, if not differently specified, all the time series shown here present CCS_{SCEN} .

Horizontal spatial averages are computed considering the sub-basins defined in Fig. 1, the whole Mediterranean

basin scale, and two macroareas: the Western Mediterranean (WMED, which includes ALB, SWM, NWM and TYR) and the Eastern Mediterranean (EMED, which includes ION and LEV). The Adriatic and Aegean seas are usually not considered part of the Eastern Mediterranean due to the importance of local forcing, such as riverine loads, in shaping the variability of the biogeochemical dynamics in those two sub-basins. Because of this, following the approach already adopted in previous works (Lazzari et al., 2012, 2016; Di Biagio et al., 2019; Reale et al., 2020a, b), they are not considered in the spatial averages related to WMED and EMED.

Temporal averages of the climate change signals are computed over two 20 year periods: 2040–2059, hereafter referred to as the “MID-FUTURE,” and 2080–2099, hereafter referred to as the “FAR-FUTURE” (Fig. S1). The relative climate change signals (in %, except for pH, which is measured in units of pH) in the MID-FUTURE or FAR-FUTURE periods with respect to the PRESENT are computed as

$$U_{\text{MID-FUTURE}} = 100 \cdot (U_{\text{SCEN-MID-FUTURE}} - U_{\text{SCEN-PRESENT}}) / U_{\text{SCEN-PRESENT}} \quad (3)$$

$$U_{\text{FAR-FUTURE}} = 100 \cdot (U_{\text{SCEN-FAR-FUTURE}} - U_{\text{SCEN-PRESENT}}) / U_{\text{SCEN-PRESENT}}, \quad (4)$$

where $U_{\text{SCEN-MID-FUTURE}}$, $U_{\text{SCEN-FAR-FUTURE}}$ and $U_{\text{SCEN-PRESENT}}$ are the averages of $U(k)_{\text{SCEN}}$ for the MID-FUTURE, FAR-FUTURE and PRESENT periods, respectively. Hereafter, if not differently specified, all the percentages shown in the maps represent $U_{\text{MID-FUTURE}}$ and $U_{\text{FAR-FUTURE}}$. The statistical significance of the relative climate change signals at each point in the basin is assessed by means of the Mann–Whitney test with $p < 0.05$.

3 Results

3.1 Evaluation of the MFS16-OGSTM-BFM control simulation for the present climate

The MFS16 modeling system performance under the present climate conditions was previously analyzed (Lovato et al., 2013; Galli et al., 2017), and it was found that the main spatiotemporal characteristics of the Mediterranean Sea physical properties compared reliably with ocean reanalysis datasets. Moreover, the physical reanalysis dataset produced by MFS16 within the Copernicus Marine Environmental Monitoring Service (CMEMS, Simoncelli et al., 2019) has already been coupled to the transport-reaction model OGSTM-BFM to carry out a reanalysis of the Mediterranean Sea biogeochemistry (Teruzzi et al., 2019). The latter is a biogeochemical dataset covering the 1999–2015 period at $1/16^\circ$ resolution, which had already been used for validating different biogeochemical simulations in the Mediterranean Sea, such as those based on the MEDMIT12-BFM

(Mediterranean MIT General Circulation Model–BFM at $1/12^\circ$; Di Biagio et al., 2019) and RegCM-ES (Regional Climate Model–Earth System; Reale et al., 2020a) modeling systems. This dataset has been recently upgraded, thus refining the resolution to $1/24^\circ$ and extending the period to 2019 (Teruzzi et al., 2021; Cossarini et al., 2021).

To date, no future climate biogeochemical projection for the Mediterranean Sea has been performed through this offline coupling.

Figure 2a, b shows the surface average Chl-*a* concentrations (upper 10 m) from the CTRL run compared with a climatology based on satellite data available from CMEMS, which covers the period 1999–2015 (Colella et al., 2016). The model correctly reproduces the areas in the Mediterranean region characterized by relatively high values of Chl-*a*: the Alboran Sea, the Gulf of Lion, the coastal areas of the Adriatic Sea and the Strait of Sicily. Moreover, the CTRL simulation captures the west–east trophic gradient of Chl-*a*, whose existence has been pointed out in previous works (D’Ortenzio and Ribera d’Alcala, 2009; Lazzari et al., 2012; Colella et al., 2016; Richon et al., 2019; Di Biagio et al., 2019; Reale et al., 2020a). On the other hand, a general underestimation by approximately 50 % of the Chl-*a* signal throughout the basin and in the coastal areas is observed, which is probably associated with an insufficient river load (Richon et al., 2019; Reale et al., 2020a) and with the tendency for satellite Chl-*a* measures to be systematically overestimated in the coastal areas with respect to in situ observations due to the presence of particulate suspended matter in the water column (Claustre et al., 2002; Morel et Gentili, 2009).

Figure 2 also shows the average vertical profiles, computed for the entire, Western and Eastern Mediterranean basins, of Chl-*a* (c), PO₄ (d), NO₃ (e), dissolved oxygen (f), DIC (g), pH (h) and ALK (i) in the CTRL compared with the recent CMEMS reanalysis (only for Chl-*a* and pH, Cossarini et al., 2021) and EMODnet (European Marine Observation and Data Network; Buga et al., 2018) datasets. In spite of the tendency to overestimate the Chl-*a* values, the model captures the DCM location, the west–east trophic gradient in the basin, the deepening of the nutricline depths between the Western and Eastern basins, and the low nutrient surface concentrations. Mean simulated values in the first 0–200 m are quite realistic for almost all the biogeochemical tracers and properties, with correlation values between the observations and modeled data of greater than 0.93. At the same time, the CTRL overestimates the PO₄ concentration between 100 and 300 m by about 50 % and the dissolved oxygen concentration by about 15 % below 200 m, and it underestimates the NO₃ concentration below 200 m by about 20 % and the pH by about 1 % between 100 and 300 m. It is worthwhile to point out that the limited spatial resolution of the observations below 200 m could impact the robustness of our comparison. In general, the biases in the initial conditions are originated by the spin-up simulation, which allows the largest part of

the model drift to be removed. As explained in Sect. 2.4, these biases, which are still present in both the CTRL and scenario simulations, do not affect the calculation of the climate change signals and are generally lower than the changes observed in the scenarios at the end of the century.

To summarize, although the model shows some deficiencies in simulating the vertical distributions of some biogeochemical tracers and properties, the main features of the system are reliably simulated and thus MFS16-OGSTM-BFM is robust enough to be used to investigate the evolution of the Mediterranean biogeochemistry under different emission scenarios.

3.2 Evolution of the thermohaline properties and circulation of the Mediterranean Sea in the 21st century

The evolution of the mean temperature and that of the salinity between 0–100 and 200–600 m in the 2005–2099 period under the RCP4.5 and RCP8.5 scenarios in the whole Mediterranean Sea and in the Western and Eastern basins are shown in Fig. 3. Just as for the biogeochemical variables, these depths have been chosen as they are representative of the locations of MAW and LIW, respectively.

A warming of the surface and intermediate layers is observed at the basin scale and in both the Western and Eastern basins. The magnitude of this warming (approximately 1.5°C in the RCP4.5 and 3°C in the RCP8.5 scenario) agrees with what has already been observed in recent modeling studies based on single/multimodel ensembles (e.g., Adloff et al., 2015; Soto-Navarro et al., 2020).

Similar to the seawater temperature, the variation in salinity is strongly dependent on the emission scenario, with more intense anomalies – both negative and positive – obtained under RCP8.5 conditions (as observed in previous modeling studies such as Adloff et al., 2015 and Soto-Navarro et al., 2020). For example, the salinity in the surface layer at basin scale and in the Eastern Basin is characterized by a decrease between 2020 and 2050 followed by a constant increase (stronger under the RCP8.5 scenario) until the end of the 21st century. Conversely, after 2050, the Western Basin shows a freshening of the surface layer with respect to the beginning of the century, in agreement with what was observed by Soto-Navarro et al. (2020). An increase in salinity also occurs in both scenarios in the intermediate layer at the basin scale and in the two main sub-basins.

The spatial distribution of temperature variations in the surface layer (Fig. S2) shows comparable and mostly statistically significant basin-scale warming in RCP4.5 and RCP8.5 in the MID-FUTURE (the differences between the projected changes are lower than 2 %), while, in the FAR-FUTURE, the projected changes in RCP4.5 are approximately 50 % lower with respect to those observed in RCP8.5 (8%–12 % and 17%–20 % respectively), with the North Western Mediterranean, Tyrrhenian, Adriatic, Ionian, Aegean Sea and

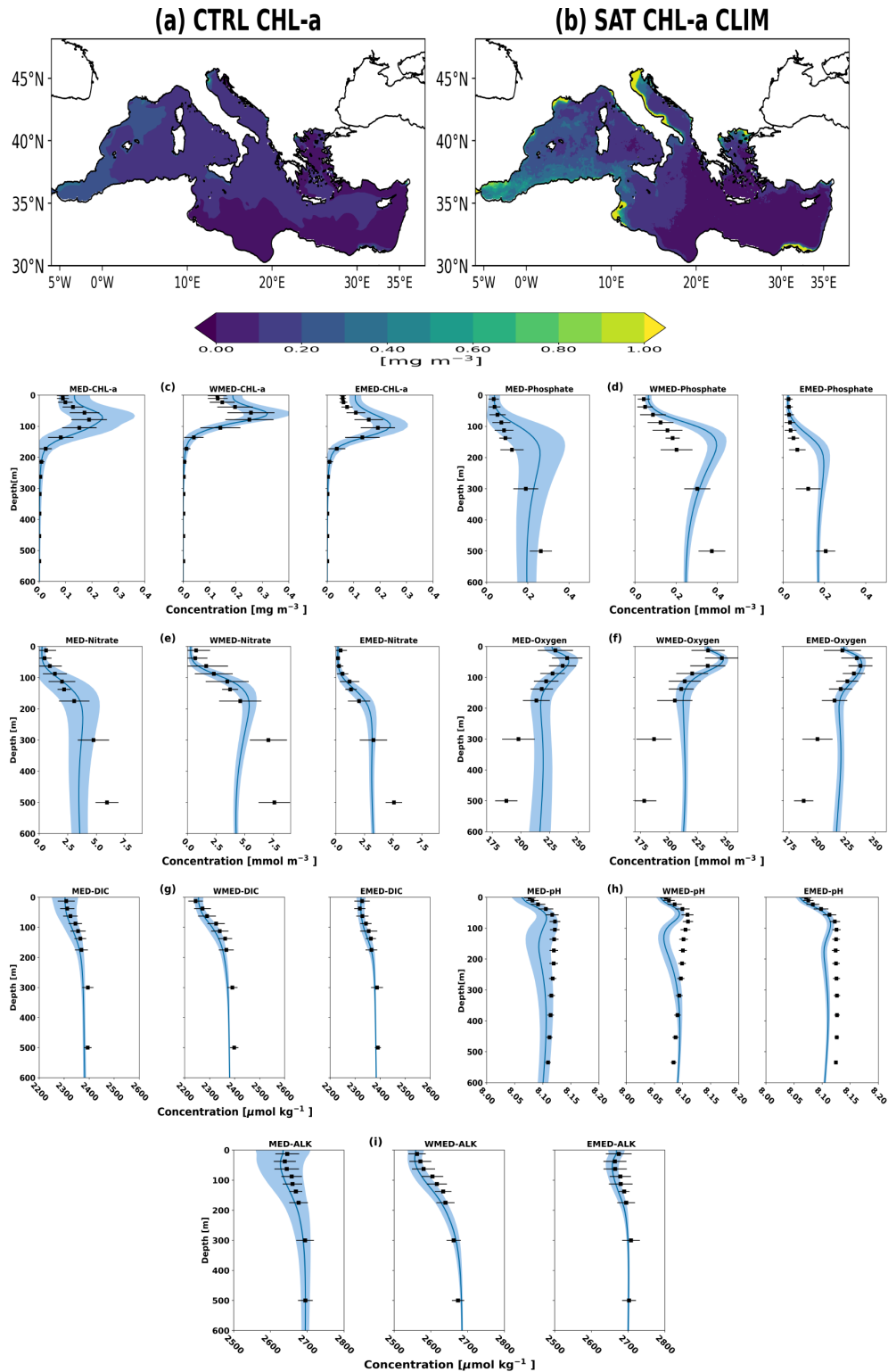


Figure 2. Average Chl-*a* in the first 10 m in CTRL for the period 2005–2020 (a) and CMEMS-SAT (b), together with CTRL average vertical profiles (blue lines) for the period 2005–2020 of Chl-*a* (c, mg m^{-3}), PO_4 (d, mmol m^{-3}), NO_3 (e, mmol m^{-3}), dissolved oxygen (f, mmol m^{-3}), DIC (g, $\mu\text{mol kg}^{-1}$), pH (h) and ALK (i, $\mu\text{mol kg}^{-1}$). The averaged profiles are computed for the entire (MED), the Western (WMED) and the Eastern (EMED) Mediterranean Sea. The light blue areas represent the spatial standard deviation of the monthly model data. The model data are compared with CMEMS reanalysis (Chl-*a* and pH; Colella et al., 2016; Teruzzi et al., 2021) and observations provided by EMODnet (PO_4 , NO_3 , dissolved oxygen, DIC, ALK; Buga et al., 2018): annual means (black squares) and related standard deviations (black bars). Depths are measured in meters.

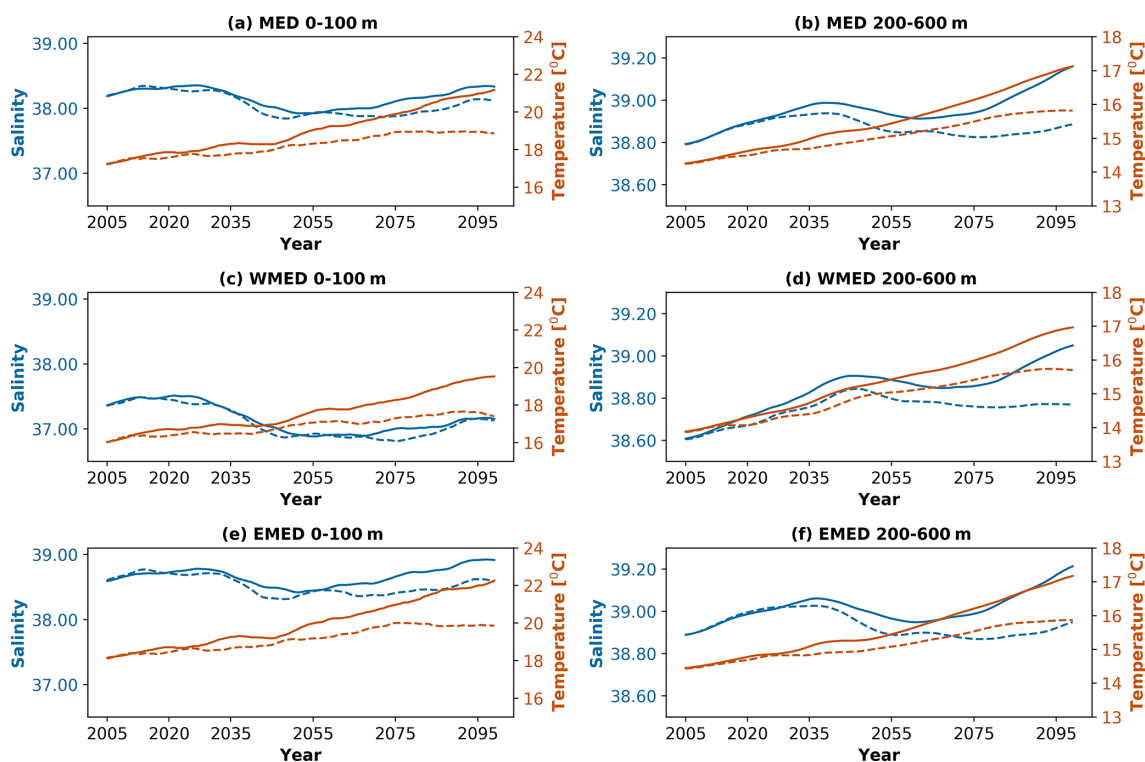


Figure 3. Yearly time series for the period 2005–2099 of salinity (blue) and temperature (dark orange, in °C) under the emission scenarios RCP8.5 (solid lines) and RCP4.5 (dashed lines) in the Mediterranean Sea (MED, **a–b**), Western Mediterranean (WMED, **c–d**) and Eastern Mediterranean (EMED, **e–f**) for the 0–100 m (**a, c, e**) and 200–600 m (**b, d, f**) layers. The yearly time series have been smoothed using the 10-year running mean.

Levantine being the most affected sub-basins. Local relative maxima are observed in both scenarios, in the Gulf of Lion, in the relatively shallow and coastal areas of the Adriatic Sea, and in the area of the Rhodes Gyre (Fig. S2i, j).

A general freshening of the upper layers and salting of the intermediate layers over most of the Mediterranean basin is observed during the MID-FUTURE period (Fig. S3). The projected changes are statistically significant over most of the basin, with the only exceptions, in both scenarios, being the upper layers of the Adriatic Sea and northern Ionian Sea and the intermediate layers of the southern Ionian Sea, the Levantine Basin/southern Adriatic Sea and the northern Ionian Sea in the RCP4.5/RCP8.5 scenarios, probably as a consequence of the river input to the Adriatic Sea and Mid-Ionian Jet dynamics. The latter has been recognized, in fact, as being an important driver of the salinity in the upper and intermediate layers of the Adriatic and Ionian seas (e.g., Gačić et al., 2010). In the FAR-FUTURE, the freshening of the surface is still present at the basin scale in the RCP4.5 scenario (although it is reduced with respect to the MID-FUTURE), and in the Western Basin in the RCP8.5 scenario. Moreover, an increase in salinity is observed in the Adriatic Sea and in the Eastern Basin under RCP8.5. The projected changes in surface salinity in the Adriatic Sea and the northern Ionian Sea under RCP4.5 are also not significant.

The decrease in salinity in the 21st century in the Western Basin is driven by the salinity values imposed in the Atlantic buffer zone (Lovato et al., 2013), while the salting of the Eastern Basin under the RCP8.5 scenario is linked to the decreasing freshwater discharge in the area (e.g., Gualdi et al., 2013; Soto-Navarro et al., 2020). In the intermediate layer, the situation is reversed: while the entire basin experiences an increase in salinity associated with the increase in salinity in the surface water of the Eastern Basin in RCP8.5, in RCP4.5, the Eastern Basin experiences a slight decrease in salinity associated again with the freshening of surface water. In fact, at the surface, both signals are transported by vertical mixing to the intermediate layers of the Eastern Basin, influencing the salinity of the newly formed LIW.

Figure 4 shows the temporal evolution of the Mediterranean thermohaline circulation during the 21st century using the zonal overturning stream function (or ZOF; Myers and Haines, 2002; Somot et al., 2006). The ZOF was computed by meridional integration of the zonal velocity from south to north and from the bottom to the top of the water column (see Adloff et al., 2015). The domain of the integration is the same as shown in Fig. 1, with the exclusion of the Atlantic area outside the Strait of Gibraltar. The thermohaline circulation of the basin in the PRESENT is composed of two cells, similar to the outcomes of the historical reference

experiments described in Adloff et al. (2015) and Waldman et al. (2018). The first cell extends from the surface to 800 m, with a clockwise circulation associated with MAW moving eastwards and LIW moving westwards. The second cell is located between 500 and 2500 m in the Eastern Mediterranean, and has a counterclockwise circulation associated with the Eastern Mediterranean Deep Water (EMDW) moving eastwards and LIW moving westwards.

Under the two scenarios, during the MID-FUTURE period, there is an evident weakening of both cells and a reduction in the thickness of the upper-layer cell and the Eastern Basin cell (less than -0.1 Sv), which splits into two subcells. By the end of the century, both cells show similar behavior, whereas in the RCP4.5 scenario, the Eastern Basin cell is slightly more intense. The weakening of the zonal overturning stream function is similar to previous findings of Somot et al. (2006) and Adloff et al. (2015). As the Mediterranean thermohaline circulation is driven by both deep and intermediate water formation processes, the overall weakening of both cells is a direct consequence of the increase in the vertical stratification of the water column. In fact, the evolution of the winter maximum mixed-layer depth in key convective areas of the Mediterranean Sea, such as the Gulf of Lion, southern Adriatic, Aegean Sea and Levantine Basin (Fig. S4), shows a progressive decrease in the intensity of open ocean convection after 2030. Only for the Aegean Sea, the changes in the winter mixed-layer maximum depth are less marked, with the occurrence of some maxima around 2080 (in RCP8.5) or after 2090 (in RCP4.5), which could correspond to a future tendency of the thermohaline circulation of the Eastern Basin to produce EMT (Eastern Mediterranean Transient)-like events (Adloff et al., 2015).

The projected overall weakening of the Mediterranean thermohaline circulation leads to a reduction in the exchanges of biogeochemical properties between the Western and Eastern basins through the Strait of Sicily at both the surface and intermediate levels (Fig. S5) and to a reduced ventilation of intermediate/deep waters (Adloff et al., 2015).

3.3 Spatial and temporal evolution of nutrients, dissolved oxygen and Chl-*a* concentrations

Figures 5 and 6 show the spatial distributions of the changes in dissolved nutrient concentrations (including both the magnitude and the sign of each change) during the 21st century. In the FAR-FUTURE, the decreases in PO_4 and NO_3 concentrations in the 0–100 m layer in RCP4.5 are almost half (approximately 7 % and 13 % for PO_4 and NO_3 , respectively) those observed in RCP8.5 (approximately 13 % and 20 % for PO_4 and NO_3 , respectively) and are particularly marked and statistically significant in the Levantine Basin, in the Aegean Sea, in the central/southern Adriatic Sea and the northern Ionian Sea. Again, areas with statistically significant maximal changes (in absolute values) are observed in both scenarios in the areas of the Gulf of Lion, Southern Adriatic, Northern

Ionian and Rhodes Gyre. Moreover, there are clear spatial gradients affecting the statistical significance of the projected changes. For example, the projected changes in nutrient concentration in the northern Adriatic Sea and in many other coastal areas (influenced by river dynamics) are not significant, contrary to what is observed in the open ocean areas of the same sub-basin. Here, the projected decrease is associated with the reduced vertical mixing in the water column and reduced inflow of nutrients through the Otranto Strait (Fig. S6). Finally, the two scenarios show some significant changes in the dissolved nutrient concentrations at a local scale in the Alboran Sea and in the southern Ionian, which are associated with changes in the intensity of mesoscale circulation (eddies) in both areas and in the intensity and spatial structure of the Mid-Ionian Jet (not shown).

In contrast to the general decreasing nutrient content of the upper layer, in both scenarios the intermediate layer shows a strong (milder) increase in nutrient concentration in the southern Aegean Sea (Levantine Basin, North Western Mediterranean and Alboran Sea) in the 21st century, driven by the reduced vertical mixing, which tends to increase the nutrient content of the intermediate layers. The Tyrrhenian, Ionian and southern Adriatic seas are, in turn, characterized by a permanent negative anomaly. In the first two areas, the anomaly can be associated with the decrease in the westward transport of nutrients in the intermediate layers through the Strait of Sicily (consequences of the weakening of the zonal stream function, as discussed in Sect. 3.2, see also Fig. S5 in the Supplement), while in the Adriatic Sea, the projected changes are driven by the increase in the nutrient export in the intermediate layer through the Otranto Strait (Fig. S6). In the North Western Mediterranean, the observed positive anomalies become weaker and even negative in the FAR-FUTURE under the RCP4.5 emission scenario, likely due to some convective events that take place between 2080 and 2100, as shown in Fig. S4. Comparing the projected changes at the surface in the FAR-FUTURE, it is observed that while they are not statistically significant in most of the Western Mediterranean and the Ionian Sea under RCP4.5, under the RCP8.5 emission scenario, statistically significant projected changes are initially limited to the Adriatic, Aegean Sea and Levantine Basin but are then also observed for the Ionian and Tyrrhenian seas.

The temporal evolution of the mean concentrations of PO_4 and NO_3 in the RCP4.5 and RCP8.5 simulations between 0–100 and 200–600 m in the Mediterranean Sea and its Western and Eastern basins for the 2005–2099 period is shown in Fig. 7. In the RCP8.5 scenario, the PO_4 and NO_3 concentrations within the euphotic layers of both sub-basins are mostly stable for the first 30 simulated years, while a marked decline occurs after 2030–2035, with values of -0.01 and -0.1 mmol m^{-3} (compared to the beginning of the century), respectively, which is followed by a steady evolution of the concentration values until the end of the century. The same behavior is observed in RCP4.5, except for a recovery that

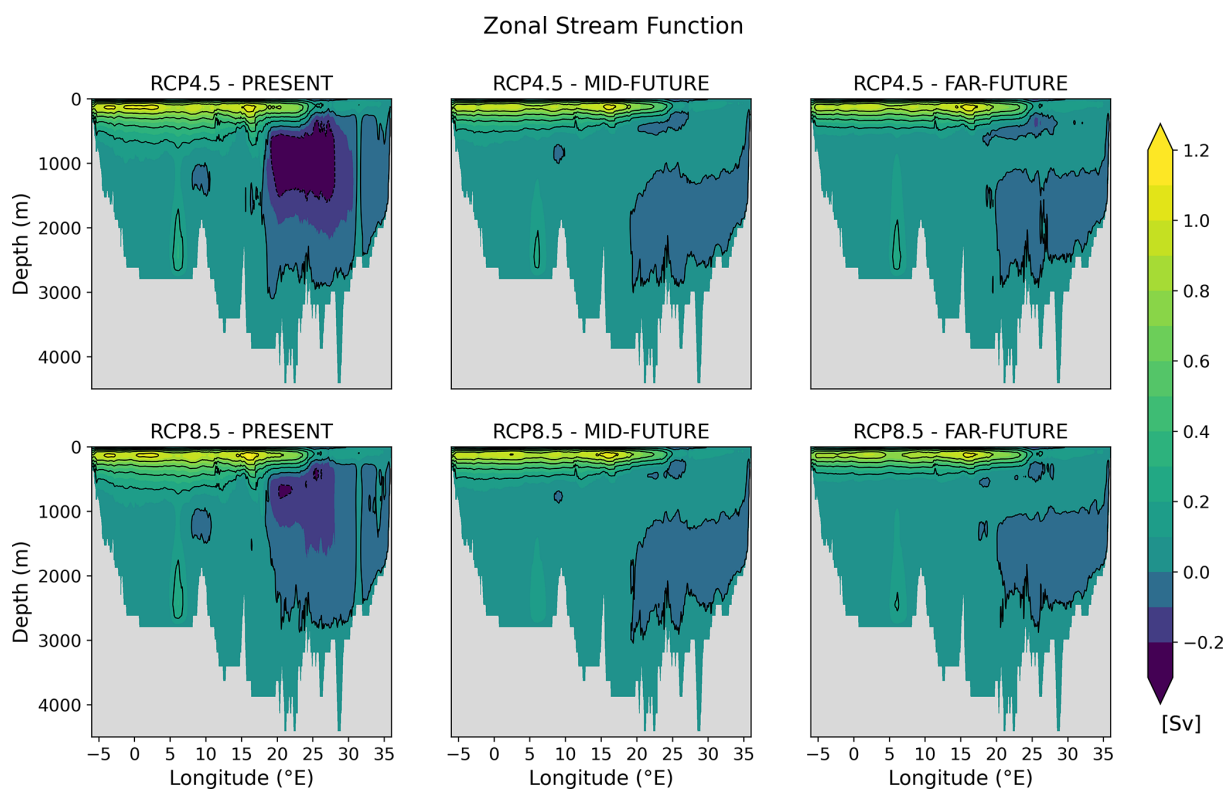


Figure 4. Mediterranean Sea zonal stream function annual mean (in Sv) averaged over the PRESENT (2005–2020), MID-FUTURE (2040–2059) and FAR-FUTURE (2080–2099) periods under the RCP4.5 and RCP8.5 scenarios.

takes place at the end of the century in correspondence to an increase in the nutrient inflow into the Alboran Sea (Fig. S7). The observed decline is temporally in phase with the weakening of the zonal stream function discussed in Fig. 4, further pointing out the importance of vertical mixing in driving the temporal variability of nutrients in the euphotic layer. From this point of view, some relative maxima in both nutrient concentrations in the Western Basin are observed for RCP4.5 in the 2015–2040 period (Fig. 7c), which are associated with strong ocean convective events taking place in the Gulf of Lion (Fig. S4). Between 2055 and 2075, for RCP4.5, the peaks in the concentrations of both nutrients temporally correspond to a peak in the inflow of nutrients into the Alboran Sea (Fig. S7). Additionally, after 2035, in both scenarios, the intermediate layer of the Western Basin presents a decrease in the nutrient concentrations (greater than 0.01 mmol m^{-3} for PO_4 and 0.1 mmol m^{-3} for NO_3), related to a reduced westward transport of nutrients associated with LIW (Fig. S5).

The temporal evolution of Chl-*a* in the two scenarios is similar to what was observed in the case of dissolved nutrients, with high interannual variability, a decrease after 2030–2035 of approximately 0.03 mg m^{-3} , and a stable signal until the end of the century in the RCP8.5 scenario, while a recovery towards the observed PRESENT values is simulated to occur at the end of the 21st century in the case of RCP4.5

(Fig. 8). In the Eastern Mediterranean, the decrease is of the same magnitude as that observed at the basin scale, while the Chl-*a* signal in the Western Basin appears mostly stable with respect to the present.

During the 21st century, a continuous decrease in the oxygen concentration in the Mediterranean Sea is projected in both scenarios (Fig. 8). The simulated reduction in the oxygen values is slower in RCP4.5 with respect to RCP8.5. For example, under the RCP8.5 emission scenario, the concentration of the dissolved oxygen in the upper layer decreases by approximately 15 mmol m^{-3} , which is three times the value observed in the RCP4.5 scenario (Fig. 8). The decrease in dissolved oxygen is rather uniform and almost statistically significant everywhere in both the horizontal and vertical directions in all the sub-basins, with values in RCP4.5 (in percentages) that are half those observed under RCP8.5 (Fig. S8). For example, the decrease in the oxygen concentration in the Levantine Basin in the FAR-FUTURE is approximately equal to 3% under the RCP4.5 emission scenario and 6% under the RCP8.5 emission scenario. In the North Western Mediterranean, these values are approximately 3% and 7%, respectively. The projected decreases in both scenarios are usually lower in the Alboran Sea and South Western Mediterranean with respect to the rest of the basin as a consequence of the damping effect driven by the oxygen values imposed at the Atlantic boundary. In fact, the advection

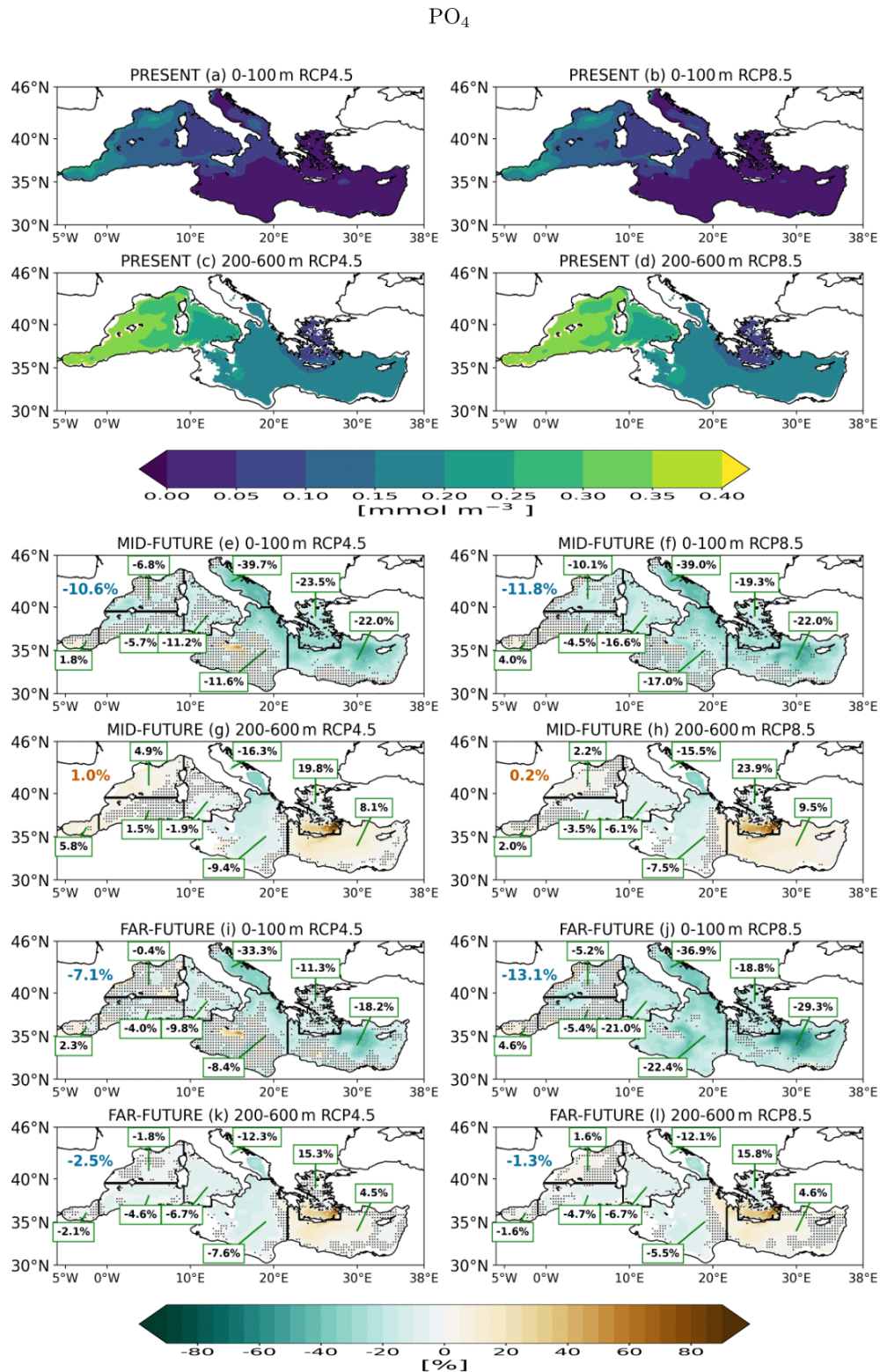


Figure 5. Phosphate concentrations (in mmol m^{-3}) in the 0–100 and 200–600 m layers in the PRESENT (2005–2020, **a, b, c** and **d**), and relative climate change signal (with respect to the PRESENT, in %) in the MID-FUTURE (2040–2059, **e, f, g** and **h**) and FAR-FUTURE (2080–2099, **i, j, k** and **l**) in the RCP4.5 (**a, c, e, g, i, k**) and RCP8.5 (**b, d, f, h, j, l**) emission scenarios. The Mediterranean average relative climate change signal in each period (with respect to the PRESENT) is displayed as a colored value (blue or dark orange when negative or positive, respectively) shown in the top left of the subfigure. Values in green boxes are the average relative climate change signals for particular periods and sub-basins shown in Fig. 1. Domain grid points where the relative climate change signals are not statistically significant according to a Mann–Whitney test with $p < 0.05$ are marked by a dot.

NO₃

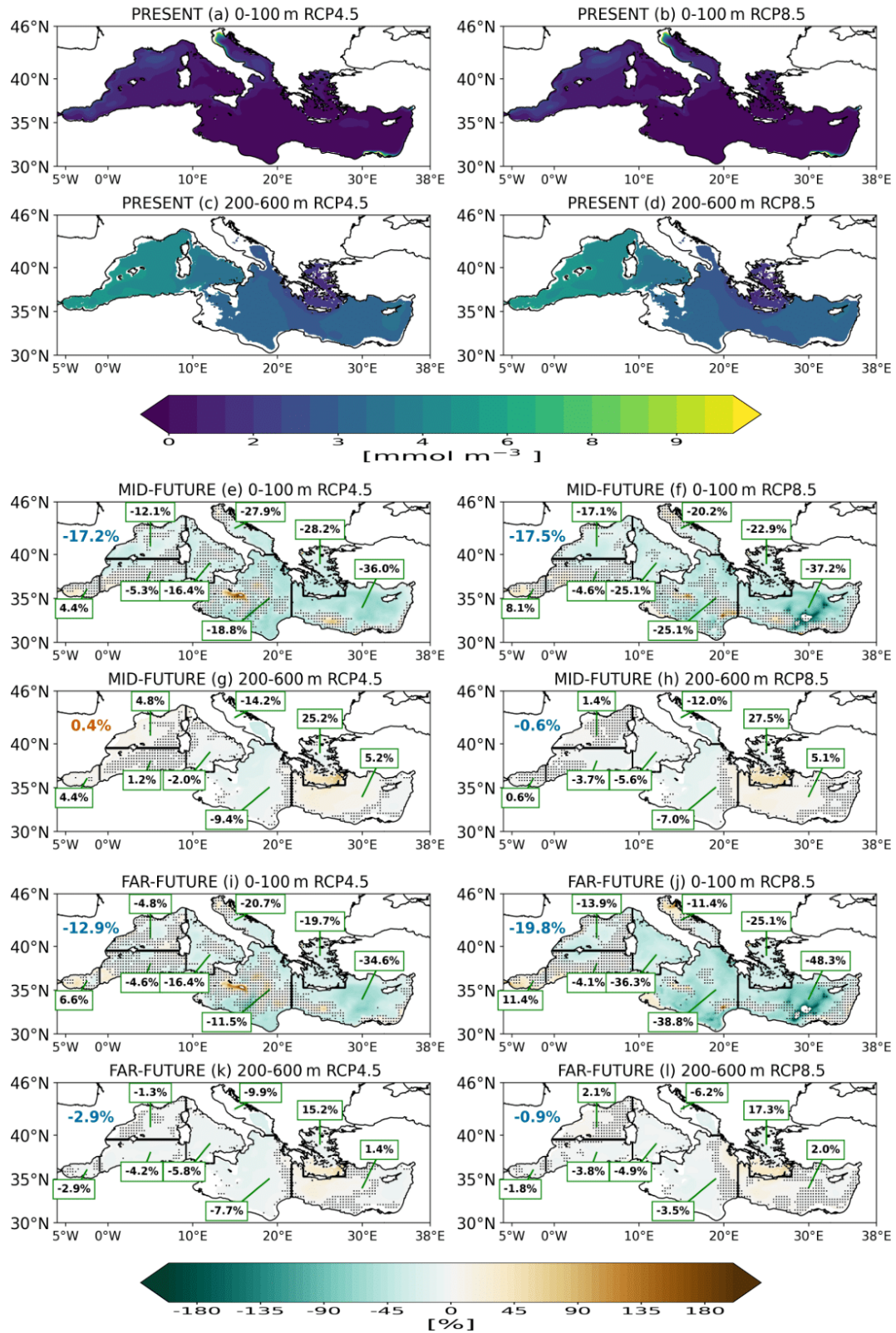


Figure 6. As Fig. 5, but for nitrate (in mmol m⁻³).

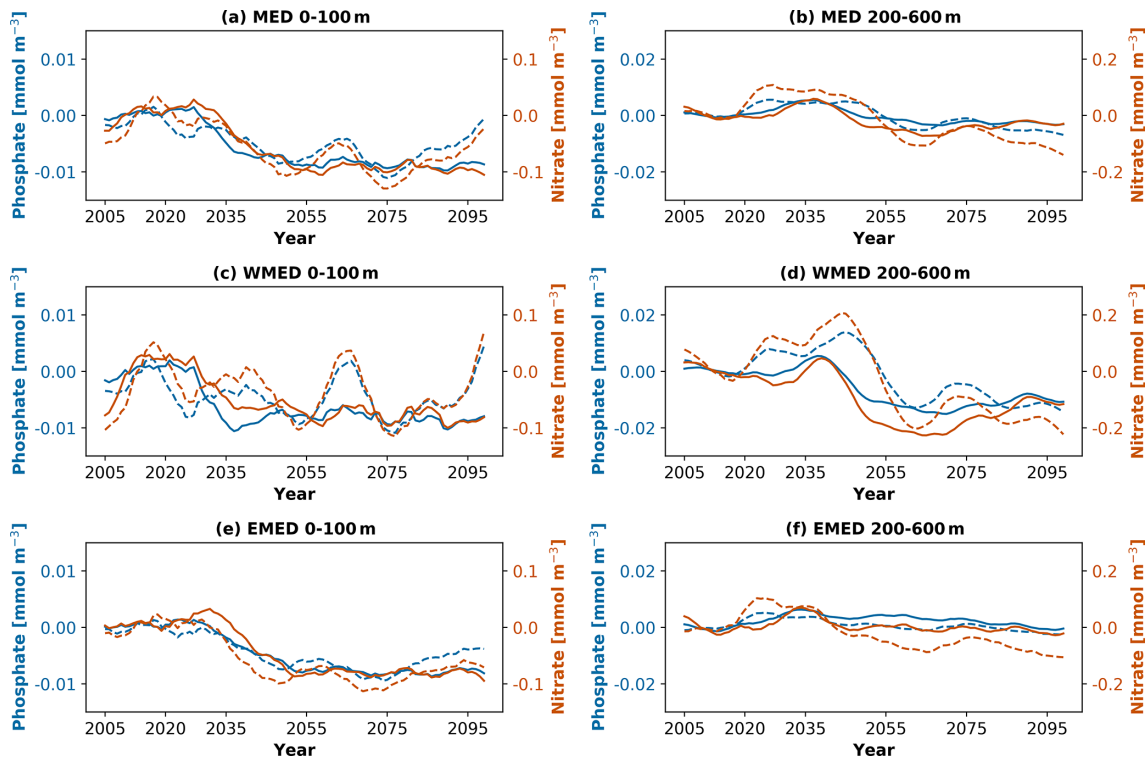


Figure 7. Yearly time series for the period 2005–2099 of phosphate (blue, in mmol m^{-3}) and nitrate (dark orange, in mmol m^{-3}) anomalies for the emission scenarios RCP8.5 (solid lines) and RCP4.5 (dashed lines) in the Mediterranean Sea (MED, a–b), Western Mediterranean (WMED, c–d) and Eastern Mediterranean (EMED, e–f) for the 0–100 m (a, c, e) and 200–600 m (b, d, f) layers. The yearly time series have been smoothed using the 10-year running mean.

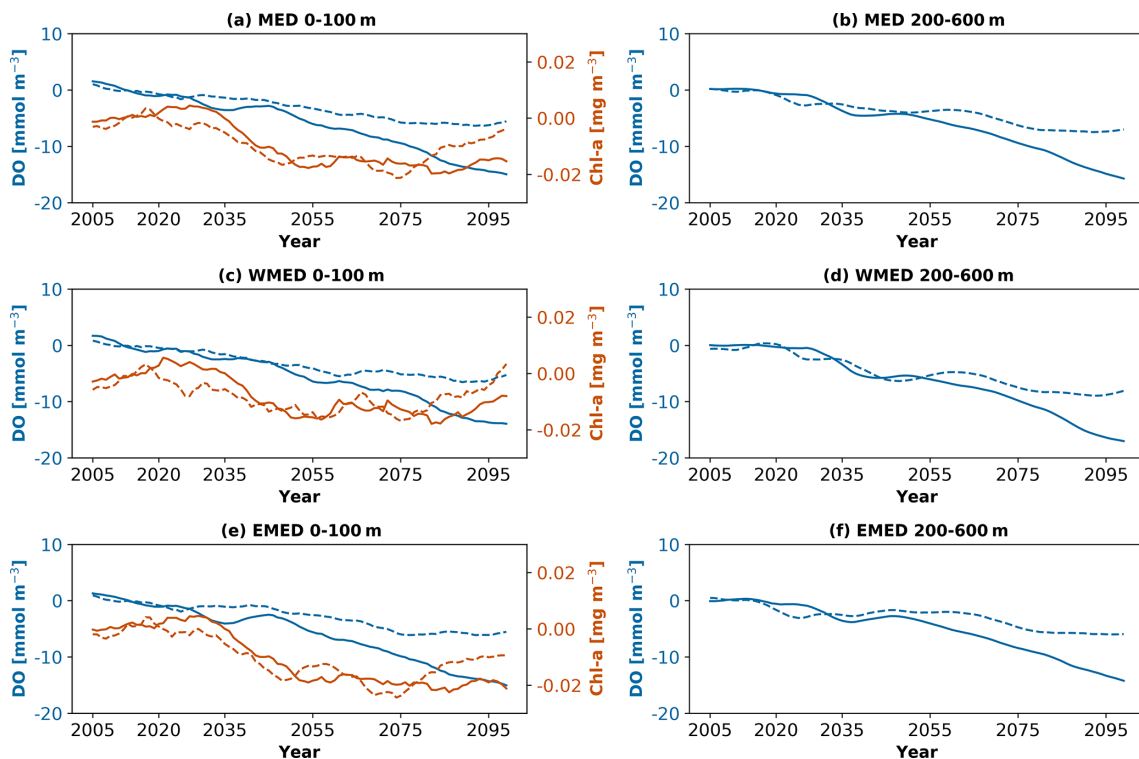


Figure 8. As Fig. 7, but for dissolved oxygen (blue, in mmol m^{-3}) and Chl-a (dark orange, in mg m^{-3}).

of dissolved oxygen associated with AW partially limits the reduction in the oxygen solubility at the surface as a consequence of the warming of the water column in the sub-basins near the Strait of Gibraltar, such as the Alboran Sea.

The uniform decrease in the oxygen surface concentration observed in Fig. S8 is spatially coherent (also from a statistical point of view) with the increase in temperature shown in Fig. S2, confirming the importance of temperature in driving the solubility of the oxygen in the marine environment (Keeling et al., 2010; Shepherd et al., 2017). Moreover, a decrease in the oxygen inflow (not shown) into the Alboran Sea and an overall increase in community respiration (see the analysis related to phytoplankton respiration in Sect. 3.4) are found, which represent additional factors explaining the projected changes. Western sub-basins, deep convection areas and shallow coastal zones of the Adriatic Sea are the regions that show the highest decreases in oxygen in both surface and intermediate layers, with the magnitude of the observed signal again depending on the considered scenario (Fig. S8) and the reduction in vertical process intensity. The effect of the increased stratification on the oxygen vertical distribution is clearly shown in Fig. 9. Under RCP8.5 (Fig. 9a, b), the progressive decline in oxygen concentration corresponds temporally to the progressive decrease in the maximum mixed-layer depth (Fig. S4) and the weakening of the zonal stream function (Fig. 4) discussed in Sect. 3.2. For example, in the North Western Mediterranean, the correlation coefficient between the average dissolved oxygen concentration in the first 100 m and the maximum mixed-layer depth has been found equal to 0.64 (statistically significant with $p < 0.05$). On the other hand, under the RCP4.5 emission scenario, some deep transport events for oxygen that lessened the decline in the oxygen concentration occur towards the end of the 21st century in both the Western and Eastern Mediterranean.

3.4 Spatial and temporal evolution of net primary production and living/nonliving organic matter

The warming of the water column and the increase in vertical stratification affect the metabolic rates of ecosystem processes, including CO₂ fixation and community respiration. In fact, a basin-wide increase in net primary production (NPP) starting after 2035 and proceeding until the end of the simulations is projected in both scenarios (Fig. 10). In the RCP4.5 scenario, the NPP increase is greater than 10 gC m⁻² yr⁻¹, which is more than half the value observed in the RCP8.5 simulation.

The distribution of the sign of the NPP change is not uniform across the basin and between the simulations (Fig. 11). In the MID-FUTURE, in both scenarios, the only areas that experience an increase (not statistically significant in all cases) in the NPP with respect to the beginning of the century are the North Western Mediterranean, the Tyrrhenian Sea, the northern Adriatic Sea, and parts of the Ionian Sea and the Levantine Basin. Conversely, the only statistically signif-

icant projected changes are negative, and they are observed in the central and southern Adriatic Sea, part of the northern Ionian Sea and the Rhodes Gyre area. The Aegean Sea shows opposite behavior, with a negative/positive anomaly observed in RCP4.5/RCP8.5. In the FAR-FUTURE, corresponding to a more pronounced warming of the basin, the NPP increase is quite uniform, statistically significant over most of the basin and approximately equal to 7 % in RCP4.5, which is approximately the half of the value observed in RCP8.5 (approximately 17 %). Under the RCP8.5 emission scenario, there is a 7 %–23 % increase in NPP throughout the basin, with relative local maxima observed mainly in the coastal areas of the North Western Mediterranean, Levantine Basin, northern Adriatic Sea, Aegean Sea (similar results, although with lower rates, were found for the end of the 21st century by Solidoro et al., 2022). Conversely, under the RCP4.5 scenario, the Adriatic Sea is still characterized by a negative and nonsignificant anomaly (−1 %), while the sign of the anomaly is positive and statistically significant for the rest of the basin, with the greatest values observed in the North Western Mediterranean (approximately 12 %, which is almost half of the variation observed in the RCP8.5 scenario). In both scenarios, a negative anomaly is observed in the Rhodes Gyre area, which is extremely weak in RCP8.5. Both negative anomalies are temporally consistent with some convective events that take place in both areas after 2080 and are shown in Fig. S4.

As shown by Lazzari et al. (2014) and Solidoro et al. (2022), the overall warming of the water column also results in an increase in community respiration. In agreement with that, Fig. S9 shows the spatial distribution of phytoplankton respiration (RESP) changes in the MID-FUTURE. It is possible to observe some differences with respect to NPP. In both scenarios, there is an overall decrease in RESP with respect to the beginning of the 21st century, which is approximately equal to −4 % in RCP4.5 and −2 % in RCP8.5. In both scenarios, the projected changes are again positive and not statistically significant in the Northern Adriatic, most of the North Western Mediterranean, the central and southern Ionian, and coastal areas of the Levantine Basin. As previously observed for NPP, the Adriatic Sea has an overall negative and statistically significant anomaly, as does the northern Ionian Sea and the area of the Rhodes Gyre. The North Western Mediterranean is the only area where the variation has the opposite sign in the two scenarios: it is negative (−1.4 %) in RCP4.5 and positive (approximately 1 %) in RCP8.5.

In the FAR-FUTURE, the pattern of variation is coherent with that already observed for the NPP (Fig. 11). RESP increases at the end of the 21st century over the entire basin by approximately 5 % (11 %) in RCP4.5 (RCP8.5). Under the RCP4.5 scenario, the Adriatic Sea (with the northern part the only exception) and the Rhodes Gyre area are still characterized by a negative anomaly, while under RCP8.5, the highest values are observed in the North Western Mediterranean (this

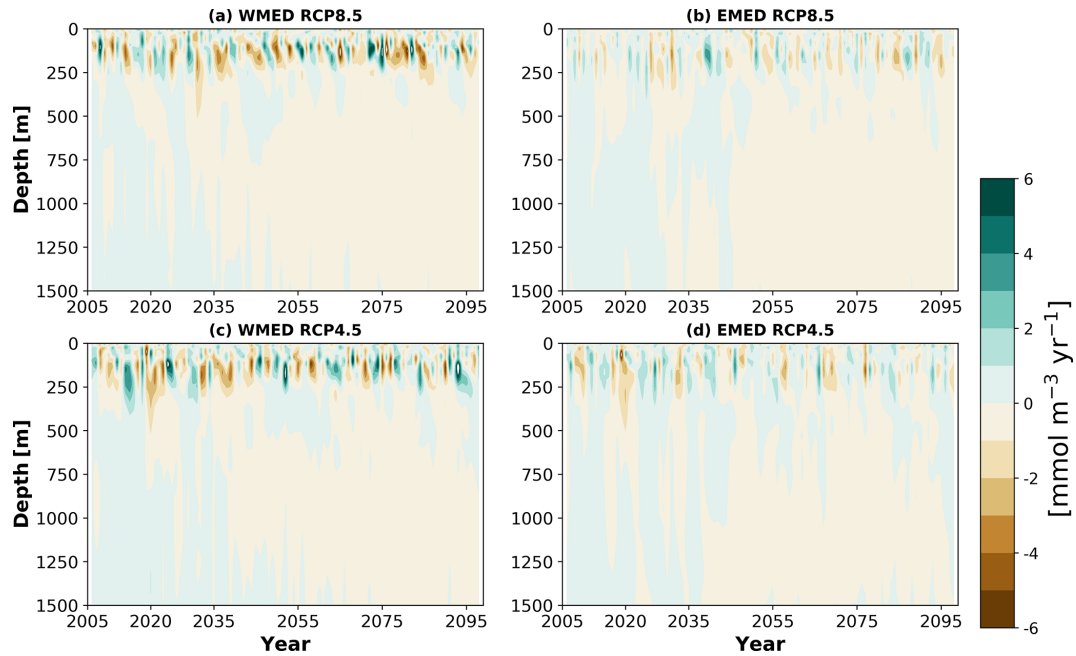


Figure 9. Annual rates of change in dissolved oxygen ($\text{mmol m}^{-3} \text{yr}^{-1}$) in the Western (a, c) and Eastern (b, d) Mediterranean Sea in RCP8.5 (a, b) and RCP4.5 (c, d).

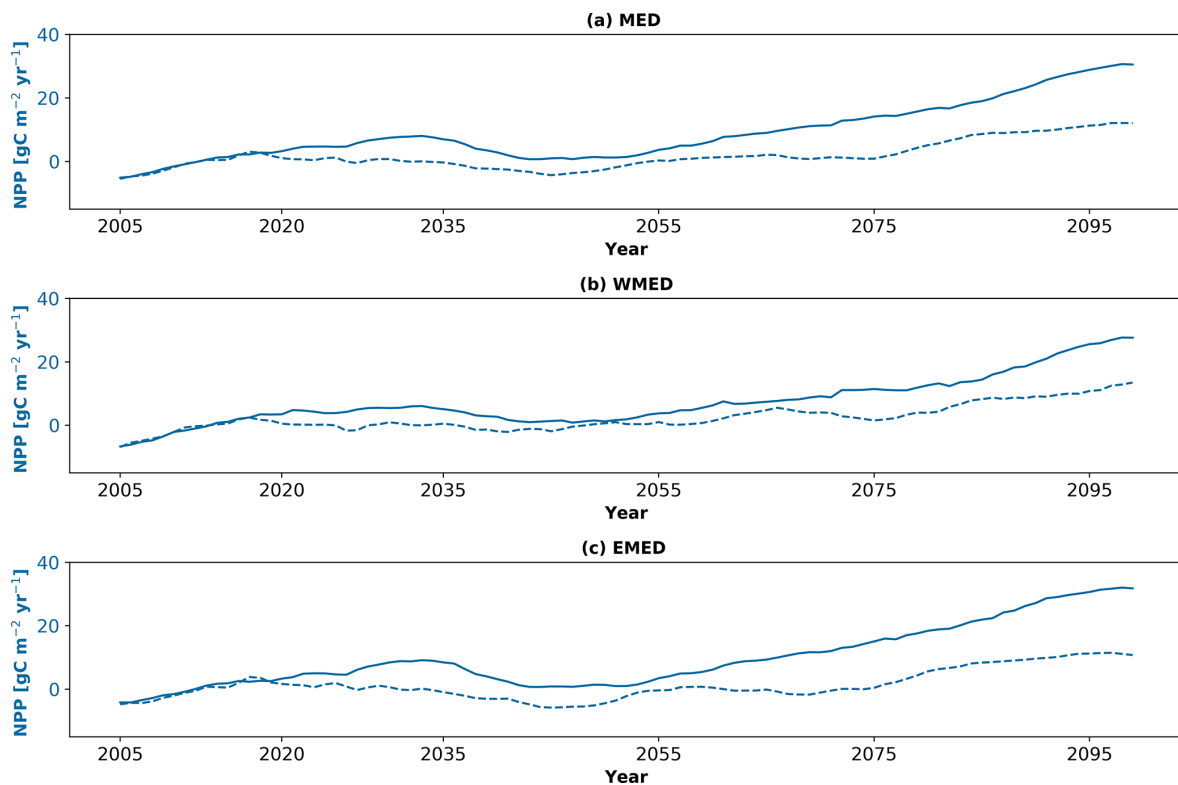


Figure 10. Yearly time series for the period 2005–2099 of integrated net primary production (blue, in $\text{gC m}^{-2} \text{yr}^{-1}$) anomalies for the emission scenarios RCP8.5 (solid lines) and RCP4.5 (dashed lines) in the Mediterranean Sea (MED, a), Western Mediterranean (WMED, b) and Eastern Mediterranean (c) for the first 200 m. The yearly time series have been smoothed using the 10-year running mean.

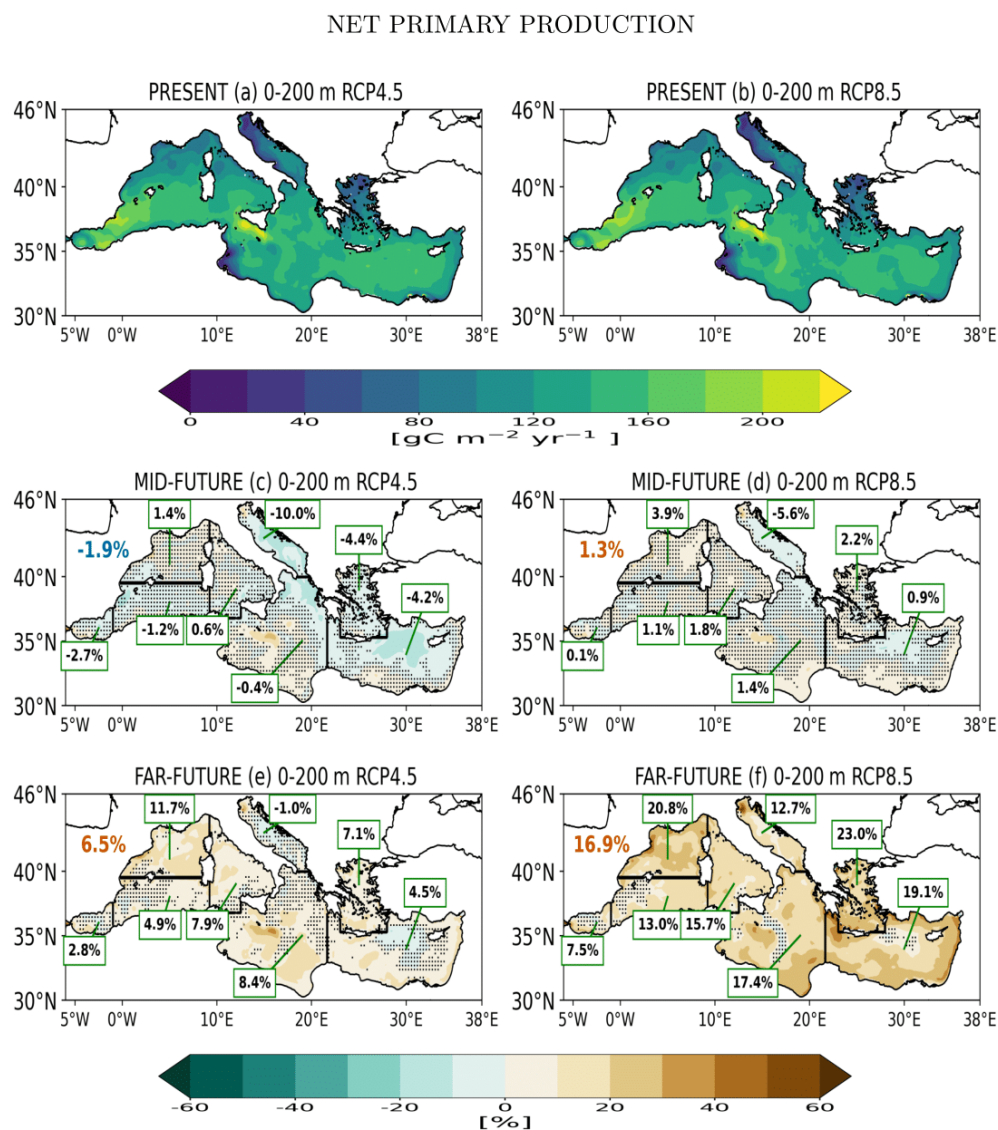


Figure 11. Integrated net primary production (in $\text{gC m}^{-2} \text{yr}^{-1}$) in the first 200 m in the PRESENT (2005–2020, **a, b**) and the relative climate change signal (with respect to the PRESENT, in %) in the MID-FUTURE (2040–2059, **c, d**) and FAR-FUTURE (2080–2099, **e, f**) in the RCP4.5 (**a, c, e**) and RCP8.5 (**b, d, f**) scenarios. The Mediterranean average relative climate change signal in each period (with respect to the PRESENT) is displayed as a colored value (blue or dark orange when negative or positive, respectively) in the top left of the subfigure. Values in green boxes are average relative climate change signals for particular periods and sub-basins shown in Fig. 1. Domain grid points where the relative climate change signals are not statistically significant according to a Mann–Whitney test with $p < 0.05$ are marked by a dot.

is also true for the RCP4.5 scenario), Aegean Sea and Levantine Basin.

A consequence of the overall increase in the respiration community is a decrease in the organic stock matter in the water column. The temporal evolution of the carbon organic matter standing stock for the 2005–2099 period in RCP4.5 and RCP8.5 simulations of the 0–100 and 200–600 m layers in the whole Mediterranean and in its Western and Eastern basins is shown in Fig. 12. The evolution of the carbon organic matter standing stock is similar to that observed for the

dissolved nutrients, with a mostly stable signal during the first 30 years of the 21st century and a decrease after 2030. Afterwards, while RCP4.5 shows a recovery at the end of the 21st century, the projected decline in RCP8.5 is approximately equal to 5 mg m^{-3} . The same dynamics are observed in the intermediate layer, where the decline after the period 2030–2035 is approximately equal to 0.3 mg m^{-3} for the carbon stock.

Similar dynamics are also observed for plankton (both phyto- and zooplankton, Fig. 13), bacterial carbon biomass

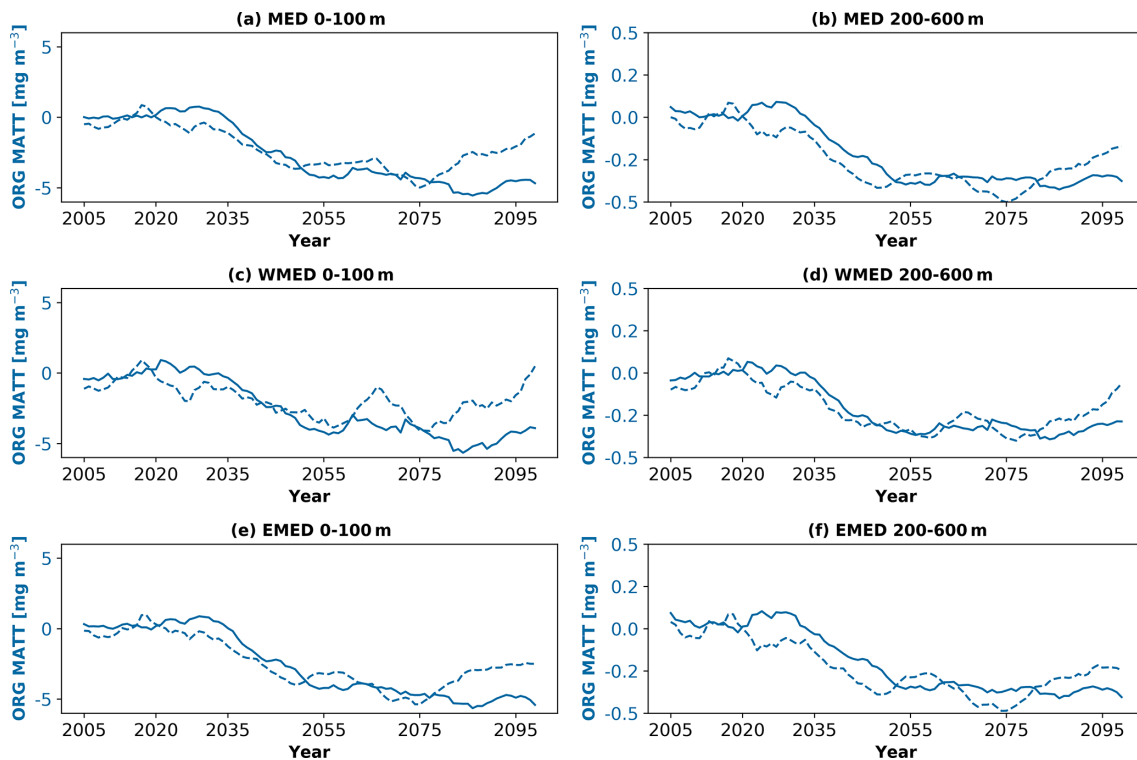


Figure 12. Yearly time series for the period 2005–2099 of living/nonliving carbon organic matter (in mg m^{-3}) anomalies for the emission scenarios RCP8.5 (solid lines) and RCP4.5 (dashed lines) in the Mediterranean Sea (MED, **a–b**), Western Mediterranean (WMED, **c–d**) and Eastern Mediterranean (EMED, **e–f**) for the 0–100 m (**a, c, e**) and 200–600 m (**b, d, f**) layers for the 2005–2099 period. The yearly time series have been smoothed using the 10-year running mean.

and particulate organic matter in the euphotic layer (Fig. 14). In the RCP4.5 simulation of all these biogeochemical tracers, a recovery in the biomass at the end of the 21st century is found, and the projected changes are approximately 50 % with respect to the RCP8.5 scenario where no recovery is observed. In particular, the decrease in the phytoplankton (zooplankton) carbon biomass is approximately 2 (1.5) mg m^{-3} , and appears to be stronger in the Eastern than in the Western Basin. Under RCP8.5, the bacterial carbon biomass is projected to decrease by the end of the century by approximately 0.5 mg m^{-3} at the basin scale, by 0.2 mg m^{-3} in the Western Basin and by 0.6 mg m^{-3} in the Eastern Basin. Finally, the decline in particulate organic matter is approximately 1.5 mg m^{-3} at the basin scale and approximately equal in the two basins. In the intermediate layer, the decline in the bacterial carbon biomass in the entire basin is fairly uniform and continuous until the end of the 21st century, with a variation of approximately 0.3 mg m^{-3} with respect to the beginning of the century. For the same layer, particulate organic matter declines after the period 2030–2035, and then the signal remains mostly stable before, in particular in the Western Basin, tending to recover at the end of the century.

In the two scenarios, in both the MID-FUTURE and FAR-FUTURE, the areas most affected by the statistically significant declines in phytoplankton carbon biomass (Fig. S10)

and zooplankton carbon biomass (Fig. S11) are mainly the sub-basins of the Eastern Mediterranean Sea, namely the Ionian Sea (mainly its northern part), the Adriatic Sea (except for its northern part), the Aegean Sea, the Levantine Basin (in particular the Rhodes Gyre area) and the Tyrrhenian Sea (only for the phytoplankton). Moreover, the negative anomaly in the area of the Rhodes Gyre is spatially coherent with the anomalies observed in the cases of the NPP and RESP, consequences of the vertical convection phenomena in the area. Conversely, positive but not statistically significant signals for both variables can be observed only at the local scale in the Strait of Sicily and along the coast of the North Western Mediterranean (spatially coherent with the positive variations in PO_4 discussed in Sect. 3.3, and not significant in either case).

Also, in the cases of bacterial carbon biomass (Fig. S12) and particulate organic matter (Fig. S13), the decline during the 21st century will mostly affect the euphotic and the intermediate layers of the Eastern Basin in both the MID- and FAR-FUTURE, with relative maxima observed in the Levantine Basin (around 33.5 % in RCP4.5 and 50 % in the RCP8.5 scenario). This decline is related to an increase in respiration at community level, as observed for phytoplankton (Fig. S9). However, there are some exceptions to the general decline in the bacterial carbon biomass and particulate organic matter

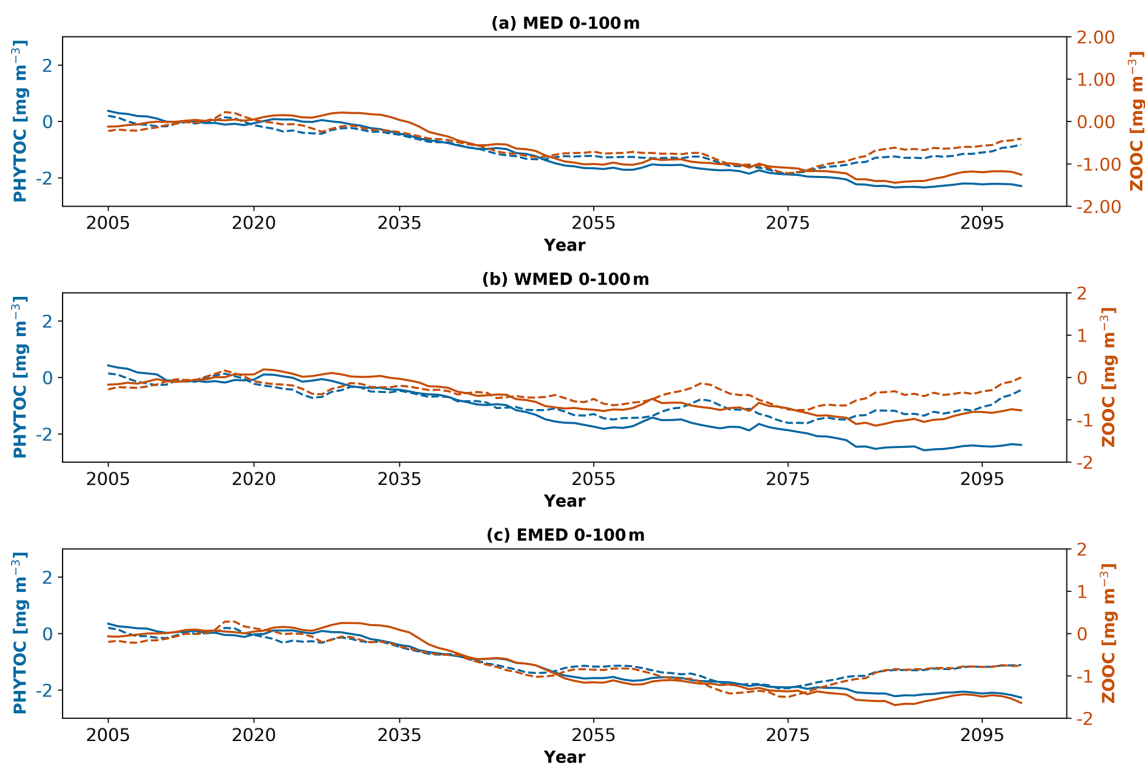


Figure 13. Yearly time series of phytoplankton carbon biomass (blue, in mg m^{-3}) and zooplankton carbon biomass (dark orange, in mg m^{-3}) anomalies for the emission scenarios RCP8.5 (solid lines) and RCP4.5 (dashed lines) in the Mediterranean Sea (MED, **a**), Western Mediterranean (WMED, **b**) and Eastern Mediterranean (**c**) for the 0–100 m layer and the 2005–2099 period. The yearly time series have been smoothed using the 10-year running mean.

in the basin. For example, in the Adriatic Sea, under scenario RCP8.5, the decrease in the bacterial carbon biomass with respect to the beginning of the century is only 1 %, with a slight positive anomaly appearing in the southern Adriatic at the end of the 21st century (not statistically significant, Fig. S12). In the case of particulate organic matter, the Strait of Sicily and the northern Adriatic Sea are characterized by a permanent positive signal in both layers and scenarios, as observed before for PO_4 and also not statistically significant in this case. Moreover, in the RCP4.5 simulation of the FAR-FUTURE period, the North Western Mediterranean shows an increase in the particulate organic matter content in the euphotic and intermediate layers.

3.5 Spatial and temporal evolution of dissolved inorganic carbon (DIC) and pH

A basin-wide continuous increase in DIC is projected until the end of the 21st century, with a stronger signal observed in the RCP8.5 scenario (Fig. 15) and, more specifically, in the eastern part of the Mediterranean Basin. In fact, the DIC increase in the euphotic layer is greater than $150 \mu\text{mol kg}^{-1}$ under RCP8.5 in the Eastern Basin, while it is greater than $120 \mu\text{mol kg}^{-1}$ in the Western Basin. Additionally, in the intermediate layer, DIC increases by $120 \mu\text{mol kg}^{-1}$ with re-

spect to the beginning of the century: this value is approximately the same for both the Western and Eastern basins and is double that observed in the RCP4.5 scenario.

Although community respiration can play a role in the increase in DIC, a predominant mechanism in the Mediterranean region is air–sea CO_2 exchange (D’Ortenzio et al., 2008; De Carlo et al., 2013; Hassoun et al., 2019; Wimart-Rousseau et al., 2020). In fact, looking at the terms controlling the DIC increase, air–sea CO_2 exchange shows an almost zero average condition in the present day (D’Ortenzio et al., 2008; Canu et al., 2015), and it increases throughout the 21st century as a consequence of the increase in atmospheric CO_2 (Fig. 16a, b). The CO_2 flux increase is almost linear and is equal in the two scenarios until 2050. Then, the RCP4.5 scenario shows a smoothing in the second half of the century, which is consistent with the reduced atmospheric emissions, while the linear increase persists under RCP8.5 (Fig. 16a, b).

The two Mediterranean sub-basins behave quite differently: the CO_2 air–sea sink is three times greater in the Western part compared to the Eastern part, reflecting the influence of both DIC and temperature spatial gradients (i.e., higher values of DIC and temperature in the Eastern Basin). In order to assess the temperature and DIC contributions to the $p\text{CO}_2$ temporal evolution, the carbonate system equations of

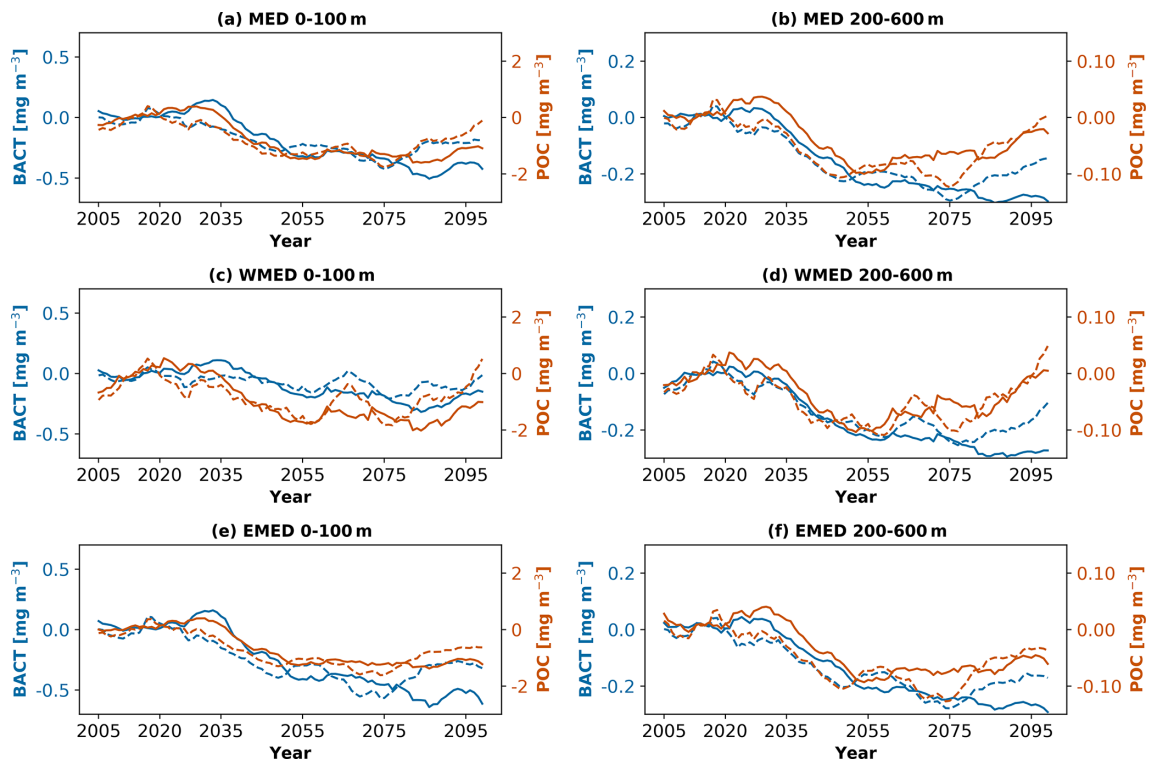


Figure 14. As Fig. 8, but for bacterial carbon biomass (blue, in mg m^{-3}) and particulate organic matter (dark orange, in mg m^{-3}).

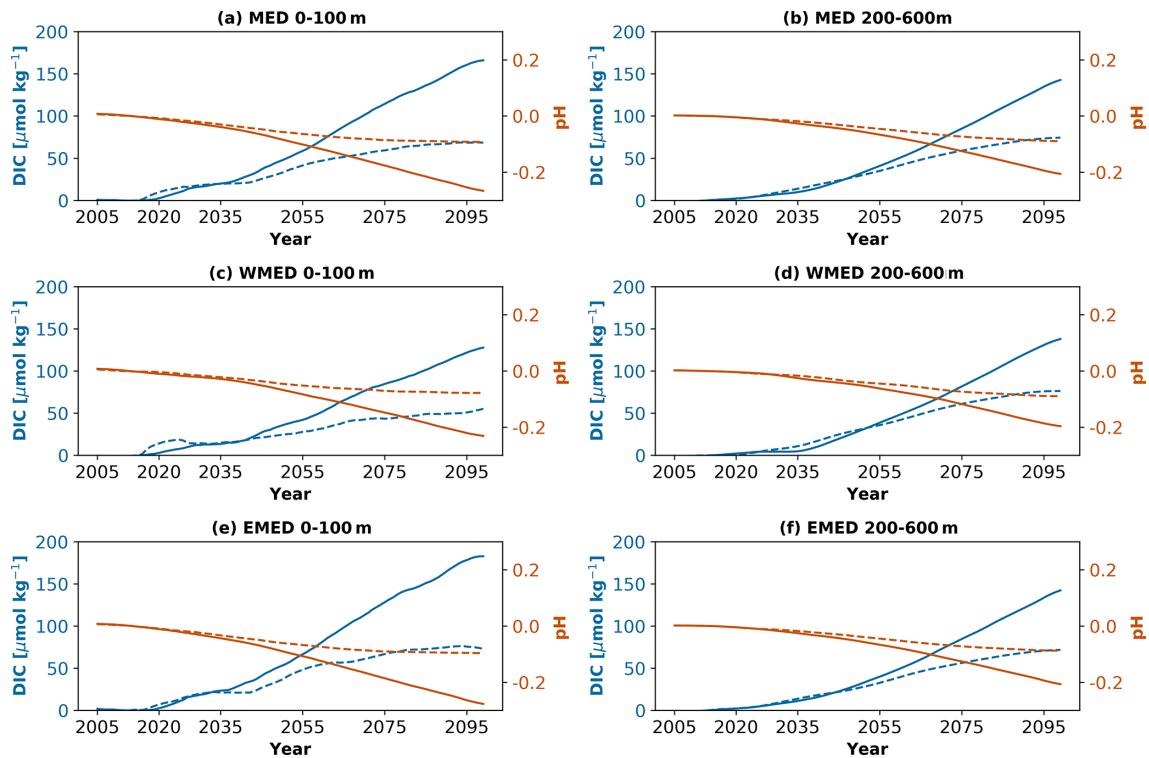


Figure 15. As Fig. 14, but for dissolved inorganic carbon (blue, in $\mu\text{mol kg}^{-1}$) and pH (dark orange).

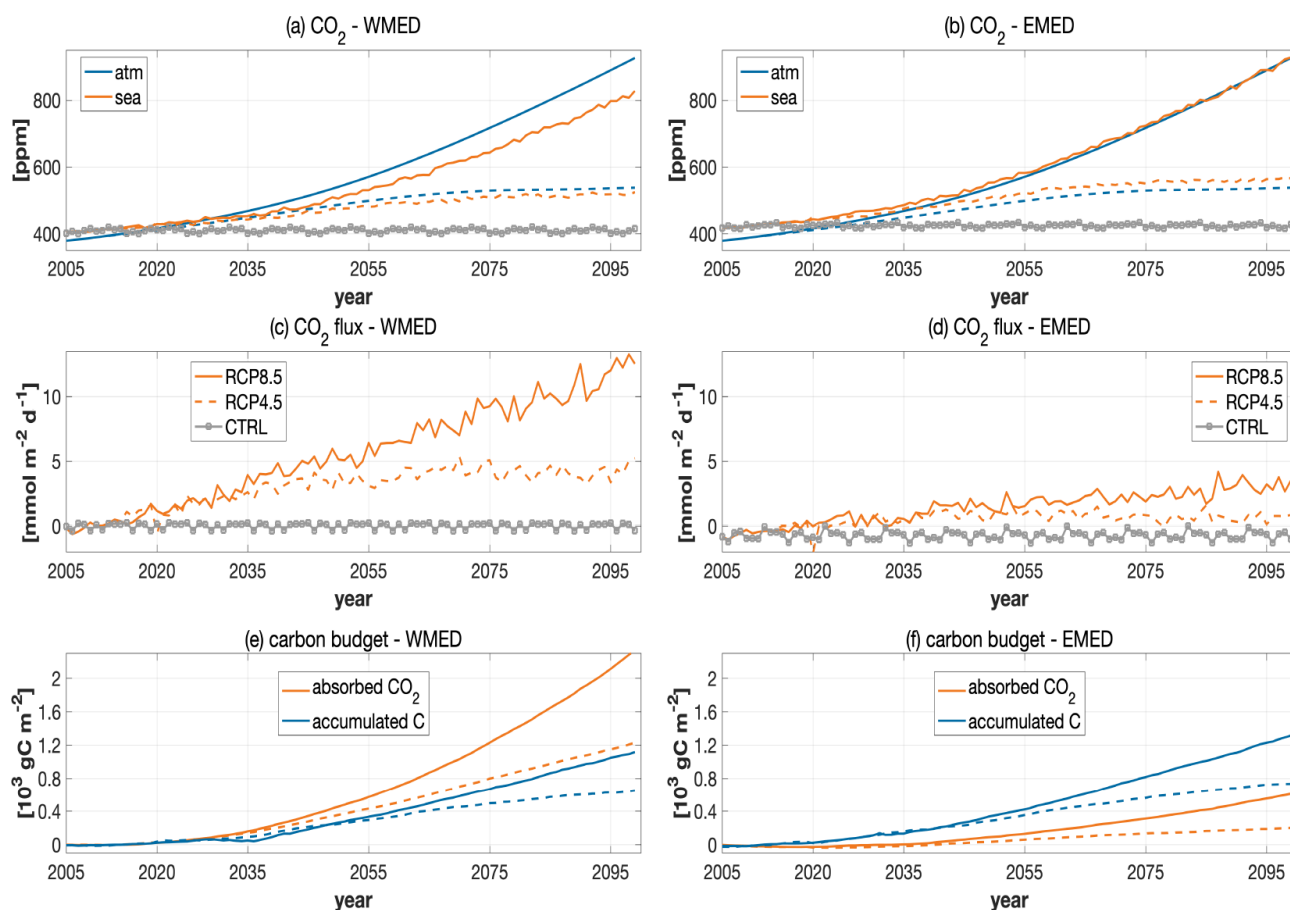


Figure 16. Time series of atmospheric and marine $p\text{CO}_2$ (a, b), CO_2 air–sea exchange (c, d) and cumulative CO_2 absorbed and accumulated in the water column (e, f) in the Western (a, c, e) and Eastern (b, d, f) Mediterranean Sea. Two scenarios – RCP4.5 (dashed lines) and RCP8.5 (solid lines) – and the control simulation (CTRL, gray lines) are reported.

the BFM model have been solved in offline mode, keeping either temperature or DIC concentration constant. The increase in the temperature has been shown to account for 25 % of the total increase in $p\text{CO}_2$. The remaining part of the $p\text{CO}_2$ increase can be ascribed to the DIC concentration increase. In the Western part, a less pronounced temperature effect (i.e., the temperature increases slower in the Western part) causes an undersaturation condition of $p\text{CO}_2$ (i.e., $p\text{CO}_2^{\text{sea}}$ is lower than $p\text{CO}_2^{\text{atm}}$) compared to the conditions in the Eastern part, triggering much higher CO_2 absorption in the Western Mediterranean.

For example, as a result of the air–sea CO_2 sink, the RCP8.5 scenario shows a steady DIC accumulation after 2030, with values of more than $2 \mu\text{mol kg}^{-1} \text{yr}^{-1}$ in the first 600 m (500 m) of the water column for the Western Basin (Eastern Basin; Fig. 17).

The increase in DIC in the upper layer is approximately 1.5 % and 2.5 % in the Western and Eastern basins, respectively, in the MID-FUTURE, and 5 % and 7 % in the FAR-FUTURE (Fig. S14). In the 200–600 m layer, the DIC increase follows the same pattern as that in the upper layer, but

with smaller changes. Then, while the DIC increase does not impact the water column below 1200 m in the Western Basin, DIC still accumulates down to 2000 m in the Eastern Basin at a rate of almost $0.5 \mu\text{mol kg}^{-1} \text{yr}^{-1}$ (Fig. 17). Occasional deep transport events for DIC can be recognized (e.g., around the years 2035, 2045, 2085 and 2095, similar to what is observed in the case of oxygen in Fig. 9), and the water column becomes enriched down to 1000–1500 m at a rate of approximately $1 \mu\text{mol kg}^{-1} \text{yr}^{-1}$. In the surface layer (i.e., the first 50–100 m), interannual variability in atmospheric conditions (i.e., specific annual wind and temperature seasonal cycles that trigger the CO_2 fluxes) and winter mixing produce an irregular succession of positive and negative annual changes which can partially hide the long-term effect of the increase in atmospheric $p\text{CO}_2$. Thus, the cumulative sum of the CO_2 absorbed through air–sea exchanges and of the carbon accumulated in the water column (Fig. 16e, f) highlight the different behaviors of the two main sub-basins. The Western Basin absorbs much more atmospheric CO_2 than the Eastern Basin, with even larger differences occurring in the RCP8.5 scenario. By the end of the RCP8.5 scenario, the cumulative

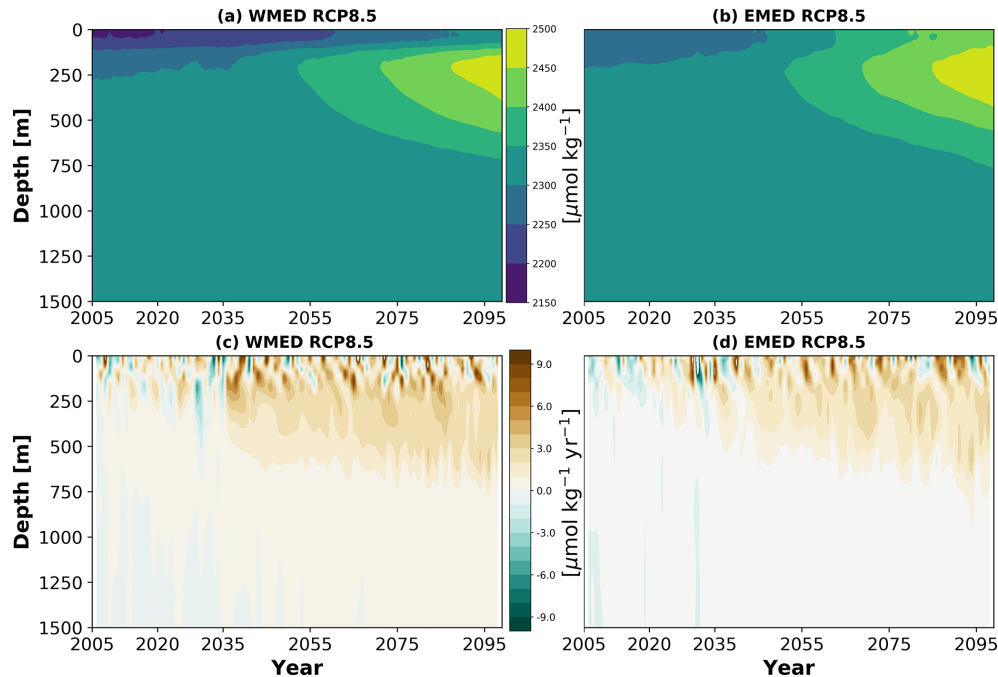


Figure 17. Hovmoeller diagrams of DIC ($\mu\text{mol kg}^{-1}$, **a, b**) and annual rates of change of DIC ($\mu\text{mol kg}^{-1} \text{yr}^{-1}$, **c, d**) in the Western (**a, c**) and Eastern (**b, d**) Mediterranean Sea in the RCP8.5 scenario.

sink of atmospheric CO_2 is 1.8 PgC in the Western Basin, while only 1 PgC is observed in the Eastern Basin, consistent with the estimates of Solidoro et al. (2022).

However, the fate of the absorbed carbon is quite different for each basin: under RCP8.5 scenario, the Western Basin accumulates only 0.85 PgC, while 1.7 PgC are retained in the water column of the Eastern Basin. As shown in Fig. 16 (lower panel) for the RCP8.5 scenario, the Eastern Basin accumulates almost 2 moles of carbon for each mole of atmospheric CO_2 absorbed, while it is less than 0.5 moles for the Western Basin. The different efficiencies are eventually triggered by the thermohaline circulation change: the Western Mediterranean carbon is partly exported to the Northern Atlantic Ocean, while an increased quota of carbon input from rivers and across the Strait of Sicily are retained in the Eastern Basin together with the atmospheric CO_2 sink after the weakening of the thermohaline circulation (Fig. 4). The RCP4.5 scenario shows similar dynamics to RCP8.5 but with the rates of CO_2 absorption (Fig. 16) and DIC accumulation almost halved and the impact of the interannual variability surface layer dynamics much more amplified (not shown). As a result, the total sequestered atmospheric CO_2 equals 0.8 and 0.25 PgC in the Western and Eastern basins, while the increase in the carbon pool is 0.5 and 0.9 PgC, respectively.

As a consequence of the CO_2 invasion and DIC increase, the change in the carbonic acid equilibrium causes a generalized decrease in pH, as also shown in Solidoro et al. (2022) in the case of the A2 scenario. The change in pH – which is statistically significant everywhere, very well anticorre-

lated in time and space with the DIC change (at the basin scale, the correlation coefficient is lower than -0.90 with $p < 0.05$; Fig. S14), and fairly similar in both the Western and the Eastern Mediterranean (as already projected by Goyet et al., 2016) – is approximately equal to 0.1 pH units in RCP4.5 and 0.25 pH units in the RCP8.5 scenario by the end of the century (Fig. 18). The largest decreases in pH are projected in both scenarios for the upper layers of the North Western Mediterranean, Tyrrhenian Sea, Adriatic Sea and Aegean Sea and in the 200–600 m layers of the Tyrrhenian Sea, Ionian Sea and Aegean Sea in the FAR-FUTURE (Fig. 18).

4 Discussions and conclusions

In this study, the coupled physical–biogeochemical model MFS16-OGSTM-BFM is used to simulate the biogeochemical dynamics of the Mediterranean Sea during the 21st century under the two emission scenarios RCP4.5 and RCP8.5, and to assess some climate change-related impacts on the marine ecosystems of the basin.

To the best of the authors' knowledge, this work is the first to analyze long-term eddy-resolving projections of the biogeochemical dynamics of the Mediterranean Sea under two different emission scenarios. In fact, the horizontal and vertical resolution ($1/16^\circ$ and 70 vertical levels) of the long-term projections analyzed here is higher than that of previous works available in the scientific literature that focus on this area (e.g., Lazzari et al., 2014; Macias et al., 2015; Richon et al., 2019; Pagès et al., 2020; Solidoro et al., 2022). Moreover,

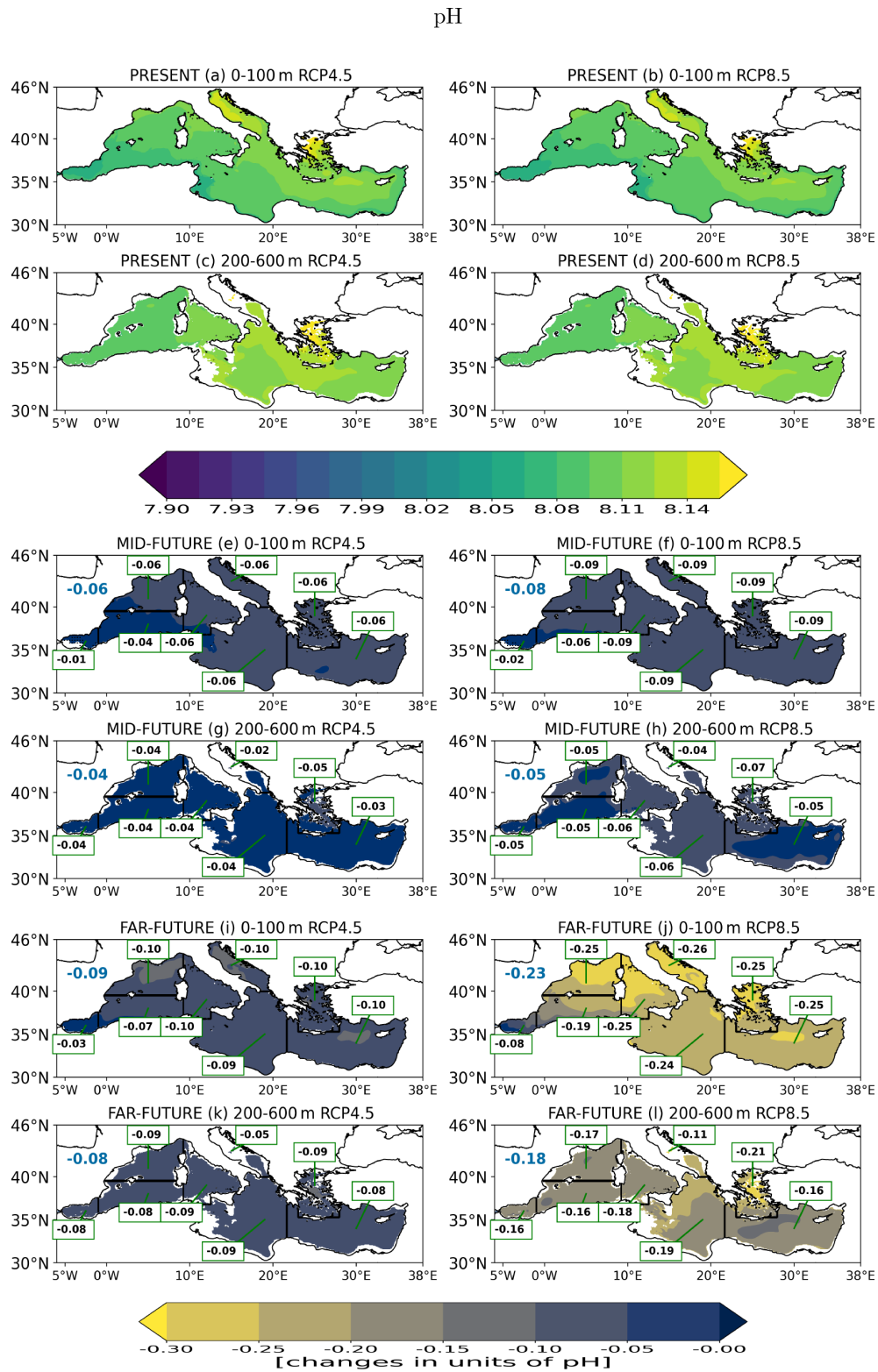


Figure 18. pH in the 0–100 and 200–600 m layers in the PRESENT (2005–2020, **a, b, c** and **d**) and relative climate change signals (with respect to the PRESENT, in units of pH) in the MID-FUTURE (2040–2059, **e, f, g** and **h**) and the FAR-FUTURE (2080–2099, **i, j, k** and **l**) in the RCP4.5 (**a, c, e, g, i, and k**) and RCP8.5 (**b, d, f, h, j** and **l**) scenarios. The Mediterranean average relative climate change signal in each period (with respect to the PRESENT) is displayed as a colored value (blue or dark orange when negative or positive, respectively) in the top left of each subfigure. Values in green boxes are the average relative climate change signals for particular periods and sub-basins shown in Fig. 1. Domain grid points where the relative climate change signals are not statistically significant according to a Mann–Whitney test with $p < 0.05$ are marked by a dot.

the majority of the recent scientific works discussing the impacts of climate change on the biogeochemical dynamics of the Mediterranean Sea are based on the analysis of simulations that consider the worst-case emission scenario (A2 or RCP8.5; Moullec et al., 2019; Richon et al., 2019; Pagès et al., 2020; Solidoro et al., 2022).

The use of eddy-resolving resolution and a higher vertical resolution allows a more detailed representation of the vertical mixing and ocean convection processes, which play a fundamental role in the ventilation of the water column and in the nutrient supply to the euphotic layer of the basin (Kwiatkowski et al., 2020). Moreover, the use of $1/16^\circ$ horizontal resolution for the projections has allowed, for the first time, spatial gradients in the same sub-basins (such as in the Adriatic Sea) or between coastal and open ocean areas (such as in the North Western Mediterranean) to be resolved, identified and characterized. A more detailed representation of the spatial distribution of the projected changes and their statistical significance for different biogeochemical tracers and properties represents a clear advantage for the future assessment of climate change impacts on specific organisms, habitats or target areas, also at the sub-basin scale.

The analysis of the thermohaline properties and circulation of the Mediterranean Sea under emission scenarios RCP4.5 and RCP8.5 found different levels of warming of the water column and weakening of the thermohaline circulation cell, with different parts of the basin being characterized by contrasting saltening and freshening conditions as a function of the considered scenario. Moreover, different levels of weakening of the open ocean convection in the most important convective areas of the basin are projected, with the only exception being the Aegean Sea, where episodes of deep convection similar to the EMT could be observed at the end of the 21st century (see also Adloff et al., 2015). All the projected changes are in agreement with those already depicted in recent modeling studies (e.g., Somot et al., 2006; Adloff et al., 2015; Waldman et al., 2018; Soto-Navarro et al., 2020).

A comparison of the model outputs with available observations together with previous studies performed with the same model system support the conclusion that the coupled model MFS16-OGSTM-BFM has a reasonably good ability to reproduce the main biogeochemical features of the Mediterranean Sea and can be used as a tool for assessing the future biogeochemical dynamics of the basin and its changes in response to climate change. The use of the bias-removing protocol is often advocated as good practice in climate studies but is rarely implemented in biogeochemical or ecosystem projections (e.g., Solidoro et al., 2022), and it adds further robustness to our results.

Our projections for the biogeochemical tracers and properties at the end of the 21st century show several signals (see Table SP1 in the Supplement for a synthetic overview) that are mostly in agreement with previous studies, at least with those based on the use of the worst-case emission scenarios. The magnitude of the projected changes has been shown to

be, in general, scenario dependent, with the largest deviations from the present climate state observed in the RCP8.5 emission scenario (Table SP1). On the other hand, the analysis of the projections obtained under RCP4.5 indicated that most of the biogeochemical variables (for example, dissolved nutrients and biomasses) had a tendency to recover the values observed in the present climate by the end of the 21st century (Table SP1).

As shown in the previous sections, by also covering the RCP4.5 scenario, our simulations highlight how an intermediate greenhouse emission scenario produces results that are not simply an average between the present condition and RCP8.5, but are (at least for some variables) something quantitatively different. For example, the temporal evolution of pH (Fig. 15) is similar in the two scenarios in the first 30 years of the 21st century. Conversely, after 2050, pH undergoes a substantial decrease under RCP8.5, while it remains almost stable under RCP4.5, with a final projected variation that is lower than half that in the worst-case scenario. This supports the idea – possibly based on the existence of a certain buffer capacity and renewal rate in a system such as the Mediterranean Sea – that the implementation of policies of reducing CO₂ emission could indeed be effective and contribute to the foundation of ocean sustainability science and policies.

The decline in the dissolved nutrients at the surface under the RCP8.5 scenario is comparable with that observed in Richon et al. (2019). However, they project an overall increase in the concentrations of both nutrients at the surface after 2050, which is ascribed by the authors to river and Gibraltar inputs that are not constant over time (as in our case) but are based on a global climate scenario simulation. As highlighted by Richon et al. (2019), the sensitivity of the biogeochemical fluxes to river loads and Gibraltar exchanges is of paramount importance and surely worthy of further investigation. Nevertheless, the increase in the concentration of nutrients in the intermediate layers of both the Western Mediterranean and the Levantine Basin can be also traced back to the reduced vertical mixing resulting from the increase in the vertical stratification (Somot et al., 2006; Adloff et al., 2015; Richon et al., 2019).

Different levels of increase in the net primary production and respiration are projected in both scenarios, although many recent studies of the Mediterranean region have shown a different response of integrated net primary production to climate change in both the Western and Eastern basins (e.g., Macias et al., 2015; Moullec et al., 2019; Pagès et al., 2020). In fact, this response may vary according to the sensitivity of the assumptions (model equations) regarding the responses of primary production and recycling processes to changes in temperature (Moullec et al., 2019). In the BFM model, temperature regulates most of the metabolic rates with a Q10 formulation (Vichi et al., 2015). The increase in net primary production is a consequence of such a dependence. In other studies (Eco3M-Med model; Pagès et al., 2020), organisms are

always optimally adapted, and no temperature dependence is accounted for in the physiology. This different parametrization could be connected to the different trend results; in fact, the scenarios based on the Eco3M-Med model result in a reduction in net primary production. In this case, surface nutrient reduction, rather than temperature, affects the net primary production trend, producing a decrease. The relative impacts of different drivers (nutrient supply versus the organism's adaptation to average water temperature) could be explored with dedicated sensitivity experiments.

Our projections of net primary production and carbon biomass dynamics show how different levels of warming of the water column and consequent stratification have a direct impact on ecosystem functioning by increasing metabolic rates. Similar to the results obtained in Lazzari et al. (2014) and Solidoro et al. (2022), the increased metabolic rates augment both primary production and respiration but have the net effect of reducing living and nonliving particulate organic matter, as suggested by theoretical considerations in O'Connor et al. (2011). The decoupled formulation of carbon uptake and net growth in the BFM model induces a further mechanism related to how carbon is channeled in the food web. In fact, the decrease in carbon biomass is partially compensated for by an increase in dissolved organic matter production in the basin by the end of the century (Solidoro et al., 2022; results not shown here).

Basin-wide deoxygenation tendencies are found in both scenarios, and are comparable to trends observed at the Mediterranean scale by Powley et al. (2016) and, under RCP8.5, at the global scale in CMIP6 (Coupled Model Intercomparison Project Phase 6; Kwiatkowski et al., 2020) simulations. The former, using a box model, found a decrease in the oxygen content of the deep layer in the range of 2%–9% as a consequence of different projected changes in the solubility (due to the temperature increase) and in the thermohaline circulation of the basin. Furthermore, the projections show that, in both our scenarios, deoxygenation is higher in the Eastern than the Western Basin, where the Atlantic boundary condition might have lessened the deoxygenation trend, and in several coastal areas such as the northern Adriatic (up to -25 mmol m^{-3}). As also observed by Powley et al. (2016), the main driver of deoxygenation is the change in solubility, whereas changes in the circulation (i.e., weakening of the thermohaline circulation) will not substantially affect deep ventilation, and it is unlikely, even in the worst-case scenario, that hypoxic conditions will be reached in the deep layer of the basin by the end of the century. On the other hand, the greatest threat to the oxygen water content might be linked to the combination of surface warming and faster respiration processes in the coastal areas of the basin, which could result in lower oxygen conditions and, thus, alteration of the local marine ecosystem functioning and structures (Bindoff et al., 2019).

An increase in the dissolved inorganic carbon content and acidity of the water column (Solidoro et al., 2022) is found

in both scenarios. The overall accumulation of CO_2 in the basin results in acidification of the Mediterranean water, with a decrease in pH of approximately 0.23 units in the worst-case scenario, which is slightly lower than the 0.3 projected at a global scale (Kwiatkowski et al., 2020) and lower than the value provided by Goyet et al. (2016), who projects, using thermodynamic equations for the CO_2 /carbonate system chemical equilibrium in seawater, a variation of 0.45 pH units in the basin under the worst SRES case scenario (and 0.25 pH units in the most optimistic SRES scenario). However, this last estimate probably tends to overestimate the future acidification of the basin, as it does not consider the decrease in the exchanges and the penetration of CO_2 across the ocean–atmosphere interface due to the warming of the water column (MedECC, 2020).

These differences in the response to climate change between the Western and Eastern basins have been also observed for the dissolved inorganic carbon accumulation, and indeed reflects different factors such as the different ventilations and residence times of the water masses in the two basins as well as the exchanges in the Strait of Gibraltar (e.g., Alvarez et al., 2014; Stöven and Tanhua, 2014; Cardin et al., 2015; Hassoun et al., 2015). Results show that, in both scenarios, the Western Basin, while adsorbing greater quantities, accumulates only half of the atmospheric carbon stored by the Eastern Basin, because the carbon in the former is partly exported to the northern Atlantic Ocean, while the carbon in the latter is also affected by a more intense reduction in the thermohaline circulation. Additionally, in our case, the use of a high resolution for the biogeochemical projections has allowed us to show that the observed acidification in many coastal areas is lower by approximately 8% with respect to that in the open ocean due to damping effects of ALK input from the rivers (not shown here).

The decline in many biogeochemical tracers and properties in the euphotic layer begins in the 2030–2035 period, in correspondence to the weakening of the thermohaline circulation in the basin (Fig. 4), and it is particularly marked in the Eastern Basin. This shows that the modification of the circulation resulting from future climate scenarios has substantial effects on the biogeochemical properties of the basin. Changes in the thermohaline circulation of the basin also explain the increase in the nutrient concentration in the intermediate layer of the Levantine Basin, which is a result of the weakening of the westward transport of nutrients through the Strait of Sicily (Fig. S5).

Similar to all previously cited modeling studies (e.g., Lazzari et al., 2014; Macias et al., 2018; Richon et al., 2019; Pagès et al., 2020), some sources of uncertainties in our projections need to be considered. As discussed before, MFS16 adequately reproduces the distribution of key physical properties and the thermohaline circulation of the basin. On the other hand, recent studies based on multimodel ensembles (Adloff et al., 2015; Richon et al., 2019; Soto-Navarro et al., 2020) have suggested that atmospheric forcing and bound-

ary conditions can strongly affect the dynamics of the basin, particularly the vertical mixing, which plays a primary role in the distribution of nutrients in the euphotic layer, therefore affecting the dynamics of low trophic levels. Additional sources of uncertainties in the modeling framework can be traced back to the BFM biogeochemical model. For instance, in the present climate, the model tends to overestimate the Chl-*a* at the surface and, even more, the oxygen concentration below 200 m (Sect. 3.1). These overestimations can be propagated by the integration into the future projections. However, the conclusions of the present work should not be significantly affected by this because, at the same time, the CTRL simulation is also removed from both the scenario simulations. Moreover, the signs of the projected changes (not their absolute values) result from different physical and biogeochemical processes (e.g., temperature and respiration increases, weakening of the thermohaline circulation, increased stratification) which are linked to the climate forcing and are independent of the model uncertainties that generate the biases discussed in Sect. 3.1.

Furthermore, the setup for the boundary conditions, namely the atmospheric deposition at the surface, the nutrient loads of rivers and the vertical profiles at the Atlantic boundary, can be very critical, especially in the landlocked Mediterranean Basin. Atmospheric deposition is an important source of nutrients for the basin, and it has been shown that the biogeochemical dynamics of the Mediterranean Sea are influenced by aerosol deposition (e.g., Richon et al., 2018, 2019), especially during periods of stratification. The projected lower nutrient supply from subsurface waters caused by climate-driven stronger stratification is likely to increase the importance of atmospheric deposition as a source of nutrients for the euphotic layer (Gazeau et al., 2021). Thus, possible future changes in the deposition of aerosols could influence the biogeochemistry of the basin and the nutrient concentrations at the surface as projected for the 21st century and depicted in Sect. 3.3. However, in both the RCP4.5 and RCP8.5 simulations, the present-day phosphate and nitrogen deposition is used. Potential improvements will be achieved by including more accurate deposition information derived from CMIP6 global estimates for the 21st century (O'Neill et al., 2016).

Similarly, the lack of river nutrient load projections under the prescribed emission scenarios can affect the projected nutrient budget of the Mediterranean Basin. A climatology derived from the Perseus project (see Sect. 2.3) is adopted here, and is, to our knowledge, the most reliable information. Indeed, it is reasonable to assume that land-use and runoff changes might impact future nutrient loads, although their magnitude and even the sign are presently unknown. Our river runoff was based on projections (Gualdi et al., 2013; Sect. 2.1) which estimated an average decrease by the end of the 21st century. Thus, the increase in nutrients observed in Figs. 9 and 10 in the northern Adriatic and several coastal areas of the Western Basin can be partially re-

lated to the mismatch between a constant nutrient load and a decreasing runoff. However, it might be worth remembering that the amount of nutrients entering the basin through its boundaries ultimately depends on economic policies and land-use/coverage scenarios and therefore may be intrinsically subjective.

With DIC as the only exception, a single vertical profile based on present-day condition data is used (i.e., no future evolution is considered) for the boundary conditions in the Atlantic for the 21st century. While this approach allows us to discern the effects of the changes in the basin circulation on the nutrient budgets, it could miss the influence on nutrients or other biogeochemical properties of a possible different future evolution of the exchanges in the Strait of Gibraltar due to changes in the tracer concentrations in the Atlantic Ocean. Moreover, the use of the same Atlantic boundary conditions for the two scenarios (Sect. 2.3) could have led to an underestimation of the potential difference between the two scenarios in the areas most influenced by the Atlantic boundary (e.g., the Alboran Sea and South Western Mediterranean). Recent physical simulations have shown an increase of 3.7 % in the surface flow at the Strait of Gibraltar, which could imply an increase in the inflow of nutrients in the surface layer at the Strait of Gibraltar (Richon et al., 2019; Pagès et al., 2020), thereby possibly damping the decrease in the nutrient concentration at the surface projected for the 21st century. As previously observed, these differences in model setup could explain the observed differences among studies that have analyzed future projections of the biogeochemistry of the basin.

To conclude, the methodology and results presented here provide a robust picture of the evolution of the Mediterranean Sea biogeochemistry for the 21st century. Clearly, the new generation of Regional Earth System coupled Models (RESMs) with eddy-resolving ocean models such as the one exploited here may partially reduce the limitations of using external (and possibly misaligned) sources of information for atmospheric and land inputs to the ocean. Indeed, by directly resolving the coupling between the Mediterranean Sea, the regional atmospheric domain and the hydrological component, a regional earth system coupled model (e.g., as used in Sitz et al., 2017; Reale et al., 2020a) allows the simulation of the different components of the climate system at the local scale, including aerosol and river loads.

Data availability. Data produced in the numerical experiments are available through the portal dds.cmcc.it for both physical (<https://dds.cmcc.it/#/dataset/medsea-cmip5-projections-physics>, Lovato, 2022) and biogeochemical (<https://dds.cmcc.it/#/dataset/medsea-cmip5-projections-biogeochemistry>, Reale et al., 2022) components.

Supplement. The supplement related to this article is available online at: <https://doi.org/10.5194/bg-19-4035-2022-supplement>.

Author contributions. GC, PL, SS, MR and CS conceived the study. They designed the experiments, together with TL. MR, GB and TL performed the numerical simulations. MR, GC, SS, TL and PL performed the analysis of the simulation results. MR prepared the first draft of the manuscript under the supervision of SS, GC, PL and CS and with contributions from TL and SM. All the authors discussed the results and contributed to the revision of the manuscript.

Competing interests. The contact author has declared that none of the authors has any competing interests.

Disclaimer. Publisher's note: Copernicus Publications remains neutral with regard to jurisdictional claims in published maps and institutional affiliations.

Acknowledgements. The CINECA consortium is acknowledged for providing computational resources through the IskraB project Scenarios for the Mediterranean Sea Biogeochemistry in the 21st Century (MED21BIO) and the IskraC DYBIO, EMED18 and MED-CLI16. This study has also been conducted using EU Copernicus Marine Service Information. The authors acknowledge Abed El Rahman Hassoun, an anonymous reviewer and the associate editor Jean-Pierre Gattuso for providing suggestions and criticisms that greatly improved the study.

Financial support. Marco Reale has been supported in this work by OGS and CINECA under HPC-TRES award number 2015-07 and by the project FAIRSEA (Fisheries in the Adriatic Region – a Shared Ecosystem Approach) funded by the 2014–2020 Interreg V A Italy–Croatia CBC Programme (standard project ID 10046951). This work has been partially supported by the Italian PRIN project ICC3 (Impact of Climate Change on the biogeochemistry of Contaminants in the Mediterranean Sea).

Review statement. This paper was edited by Jean-Pierre Gattuso and reviewed by Abed El Rahman Hassoun and one anonymous referee.

References

- Adloff, F., Somot, S., Sevault, F., Jordà, G., Aznar, R., Déqué, M., Herrmann, M., Marcos, M., Dubois, C., Padorno, E., Alcaez-Fanjul, E., and Gomis, D.: Mediterranean Sea response to climate change in an ensemble of twenty first century scenarios, *Clim. Dyn.*, 45, 2775–2802, <https://doi.org/10.1007/s00382-015-2507-3>, 2015.
- Álvarez, M., Sanleón-Bartolomé, H., Tanhua, T., Mintrop, L., Luchetta, A., Cantoni, C., Schroeder, K., and Civitarese, G.: The CO₂ system in the Mediterranean Sea: a basin wide perspective, *Ocean Sci.*, 10, 69–92, <https://doi.org/10.5194/os-10-69-2014>, 2014.
- Auger, P. A., Ulses, C., Estournel, C., Stemman, L., Somot, S., and Diaz, F.: Interannual control of plankton ecosystem in a deep convection area as inferred from a 30-year 3D modeling study: winter mixing and prey/predator in the NW Mediterranean, *Prog. Oceanogr.*, 124, 12–27, <https://doi.org/10.1016/j.pocean.2014.04.004>, 2014.
- Benedetti, F., Guilhaumon, F., Adloff, F., and Ayata, S. D.: Investigating uncertainties in zooplankton composition shifts under climate change scenarios in the Mediterranean Sea, *Ecography*, 41, 345–360, <https://doi.org/10.1111/ecog.02434>, 2018.
- Bethoux, J. P., Morin, P., Chaumery, C., Connan, O., Gentili, B., and Ruiz-Pino, D.: Nutrients in the Mediterranean Sea, mass balance and statistical analysis of concentrations with respect to environmental change, *Mar. Chem.*, 63, 155–169, 1998.
- Bindoff, N. L., Cheung, W. W. L., Kairo, J. G., Arístegui, J., Guinder, V. A., Hallberg, R., Hilmi, N., Jiao, N., Karim, M. S., Levin, L., O'Donoghue, S., Purca Cuicapusa, S. R., Rinkevich, B., Suga, T., Tagliabue, A., and Williamson, P.: Changing Ocean, Marine Ecosystems, and Dependent Communities, in: IPCC Special Report on the Ocean and Cryosphere in a Changing Climate, edited by: Pörtner, H.-O., Roberts, D. C., Masson-Delmotte, V., Zhai, P., Tignor, M., Poloczanska, E., Mintenbeck, K., Alegría, A., Nicolai, M., Okem, A., Petzold, J., Rama, B., and Weyer, N. M., Cambridge University Press, Cambridge, UK and New York, NY, USA, 755 pp., <https://doi.org/10.1017/9781009157964>, 2019.
- Buga, L., Sarbu, G., Fryberg, L., Magnus, W., Wesslander, K., Gatti, J., Leroy, D., Iona, S., Larsen, M., Koefoed Rømer, J., Østrem, A. K., Lipizer, M., and Giorgetti, A.: EMODnet Thematic Lot n° 4/SI2.749773 EMODnet Chemistry Eutrophication and Acidity aggregated datasets v2018, EMODnet [data set], <https://doi.org/10.6092/EC8207EF-ED81-4EE5-BF48-E26FF16BF02E>, 2018.
- Butenschön, M., Lovato, T., Masina, S., Caserini, S., and Grosso, M.: Alkalinization Scenarios in the Mediterranean Sea for Efficient Removal of Atmospheric CO₂ and the Mitigation of Ocean Acidification, *Frontiers in Climate*, 3, 14, <https://doi.org/10.3389/fclim.2021.614537>, 2021.
- Canu, D. M., Ghermandi, A., Nunes, P. A., Lazzari, P., Cossarini, G., and Solidoro, C.: Estimating the value of carbon sequestration ecosystem services in the Mediterranean Sea: An ecological economics approach, *Global Environ. Chang.*, 32, 87–95, 2015.
- Cardin, V., Civitarese, G., Hainbucher, D., Bensi, M., and Rubino, A.: Thermohaline properties in the Eastern Mediterranean in the last three decades: is the basin returning to the pre-EMT situation?, *Ocean Sci.*, 11, 53–66, <https://doi.org/10.5194/os-11-53-2015>, 2015.
- Claustre, H., Morel, A., Hooker, S. B., Babin, M., Antoine, D., Oubelkheir, K., Bricaud, A., Leblanc, K., Quéguiner, B., and Maritorea, S.: Is desert dust making oligotrophic waters greener?, *Geophys. Res. Lett.*, 29, 1–4, <https://doi.org/10.1029/2001GL014056>, 2002.
- Colella, S., Falcini, F., Rinaldi, E., Sammartino, M., and Santoleri, R.: Mediterranean Ocean colour chlorophyll trends, *PLoS ONE*, 11, e0155756, <https://doi.org/10.1371/journal.pone.0155756>, 2016.
- Cossarini, G., Lazzari, P., and Solidoro, C.: Spatiotemporal variability of alkalinity in the Mediterranean Sea, *Biogeosciences*, 12, 1647–1658, <https://doi.org/10.5194/bg-12-1647-2015>, 2015.

- Cossarini, G., Feudale, L., Teruzzi, A., Bolzon, G., Coidessa, G., Solidoro, C., Di Biagio, V., Amadio, C., Lazzari, P., Brosich, A., and Salon, S.: High-Resolution Reanalysis of the Mediterranean Sea Biogeochemistry (1999–2019), *Front. Mar. Sci.*, 8, 741486, <https://doi.org/10.3389/fmars.2021.741486>, 2021.
- Crise, A., Allen, J., Baretta, J., Crispi, G., Mosetti, R., and Solidoro, C.: The Mediterranean pelagic ecosystem response to physical forcing, *Prog. Oceanogr.*, 44, 219–243, 1999.
- Crispi, G., Mosetti, R., Solidoro, C., and Crise, A.: Nutrient cycling in Mediterranean basins: the role of the biological pump in the trophic regime, *Ecol. Model.*, 138, 101–114, 2001.
- Darmaraki, S., Somot, S., Sevault, F., Nabat, P., Cabos Narvaez, W. D., Cavicchia, L., Djurdjevic, V., Li, L., Sannino, G., and Sein, D. V: Future evolution of Marine Heatwaves in the Mediterranean Sea, *Clim. Dyn.*, 53, 1371–1392, <https://doi.org/10.1007/s00382-019-04661-z>, 2019.
- De Carlo, E. H., Mousseau, L., Passafiume, O., Drupp, P., and Gattuso, J. P.: Carbonate Chemistry and Air–Sea CO₂ Flux in a NW Mediterranean Bay Over a Four-Year Period: 2007–2011, *Aquat. Geochem.*, 19, 399–442, <https://doi.org/10.1007/s10498-013-9217-4>, 2013.
- Di Biagio, V., Cossarini, G., Salon, S., Lazzari, P., Querin, S., Sannino, G., and Solidoro, C.: Temporal scales of variability in the Mediterranean Sea ecosystem: Insight from a coupled model, *J. Mar. Syst.*, 197, 103176, <https://doi.org/10.1016/j.jmarsys.2019.05.002>, 2019.
- Diffenbaugh, N. S., Pal, J. S., Giorgi, F., and Gao, X.: Heat stress intensification in the Mediterranean climate change hotspot, *Geophys. Res. Lett.*, 34, GL030000, <https://doi.org/10.1029/2007GL030000>, 2007.
- D’Ortenzio, F. and Ribera d’Alcalà, M.: On the trophic regimes of the Mediterranean Sea: a satellite analysis, *Biogeosciences*, 6, 139–148, <https://doi.org/10.5194/bg-6-139-2009>, 2009.
- D’Ortenzio, F., Antoine, D., and Marullo, S.: Satellite-driven modeling of the upper ocean mixed layer and air–sea CO₂ flux in the Mediterranean Sea, *Deep-Sea Res. Pt. I*, 55, 405–434, 2008.
- Dubois, C., Somot, S., Calmanti, S., Carillo, A., Déqué, M., Dell’Aquila, A., Elizalde, A., Jacob, D., L’Hévéder, B., Li, L., Oddo, P., Sannino, G., Scoccimarro, E., and Sevault, F.: Future projections of the surface heat and water budgets of the Mediterranean Sea in an ensemble of coupled atmosphere–ocean regional climate models, *Clim. Dynam.*, 39, 1859–1884, 2012.
- Fach, B. A., Orek, H., Yilmaz, E., Tezcan, D., Salihoglu, I., Salihoglu, B., and Latif, M. A.: Water Mass Variability and Levantine Intermediate Water Formation in the Eastern Mediterranean Between 2015 and 2017, *J. Geophys. Res.-Ocean.*, 126, e2020JC016472, <https://doi.org/10.1029/2020JC016472>, 2021.
- Fedele, G., Mauri, E., Notarstefano, G., and Poulain, P. M.: Characterization of the Atlantic Water and Levantine Intermediate Water in the Mediterranean Sea using 20 years of Argo data, *Ocean Sci.*, 18, 129–142, <https://doi.org/10.5194/os-18-129-2022>, 2022.
- Foujols, M.-A., Lévy, M., Aumont, O., and Madec, G.: OPA 8.1 Tracer Model reference manual (Note du Pole de Modélisation) France, Institut Pierre-Simon Laplace (IPSL), 45 pp., 2000.
- Gačić, M., Borzelli, G. L. E., Civitarese, G., Cardin, V., and Yari, S.: Can internal processes sustain reversals of the ocean upper circulation? The Ionian Sea example, *Geophys. Res. Lett.*, 37, L09608, <https://doi.org/10.1029/2010GL043216>, 2010.
- Galli, G., Lovato, T., and Solidoro, C.: Marine Heat Waves Hazard 3D Maps and the Risk for Low Motility Organisms in a Warming Mediterranean Sea, *Front. Mar. Sci.*, 4, 136, <https://doi.org/10.3389/fmars.2017.00136>, 2017.
- Gazeau, F., Ridame, C., Van Wambeke, F., Alliouane, S., Stolpe, C., Irisson, J.-O., Marro, S., Grisoni, J.-M., De Liège, G., Nunige, S., Djaoudi, K., Pulido-Villena, E., Dinasquet, J., Obernosterer, I., Catala, P., and Guieu, C.: Impact of dust addition on Mediterranean plankton communities under present and future conditions of pH and temperature: an experimental overview, *Biogeosciences*, 18, 5011–5034, <https://doi.org/10.5194/bg-18-5011-2021>, 2021.
- Giorgi, F.: Climate change hot-spots, *Geophys. Res. Lett.*, 33, <https://doi.org/10.1029/2006GL025734>, 2006.
- Giorgi, F. and Lionello, P.: Climate Change Projections for the Mediterranean Region, *Glob. Planet Change*, 63, 90–104, <https://doi.org/10.1016/j.gloplacha.2007.09.005>, 2008.
- Goyet, C., Hassoun, A., Gemayel, E., Touratier, F., Abboud-Abi Saab, M., and Guglielmi, V.: Thermodynamic forecasts of the Mediterranean Sea acidification, *Mediterr. Mar. Sci.*, 17, 508–518, 2016.
- Gualdi, S., Somot, S., Li, L., Artale, V., Adani, M., Bellucci, A., Braun, A., Calmanti, S., Carillo, A., Dell’Aquila, A., Déqué, M., Dubois, C., Elizalde, A., Harzallah, A., Jacob, D., L’Hévéder, B., May, W., Oddo, P., Ruti, P., Sanna, A., Sannino, G., Scoccimarro, E., Sevault, F., and Navarra, A.: The CIRCE simulations: Regional climate change projections with realistic representation of the Mediterranean sea, *B. Am. Meteorol. Soc.*, 94, 65–81, <https://doi.org/10.1175/BAMS-D-11-00136.1>, 2013.
- Guyennon, A., Baklouti, M., Diaz, F., Palmieri, J., Beuvier, J., Lebaupin-Brossier, C., Arsouze, T., Béranger, K., Dutay, J.-C., and Moutin, T.: New insights into the organic carbon export in the Mediterranean Sea from 3-D modeling, *Biogeosciences*, 12, 7025–7046, <https://doi.org/10.5194/bg-12-7025-2015>, 2015.
- Hassoun, A. E. R., Gemayel, E., Krasakopoulou, E., Goyet, C., Abboud-Abi Saab, M., Guglielmi, V., Touratier, F., and Falco, C.: Acidification of the Mediterranean Sea from anthropogenic carbon penetration, *Deep-Sea Res. Pt. I*, 102, 1–15, 2015.
- Hassoun, A. E. R., Fakhri, M., Abboud-Abi Saab, M., Gemayel, E., and De Carlo, E. H.: The carbonate system of the Eastern-most Mediterranean Sea, Levantine Sub-basin: Variations and drivers, *Deep-Sea Res. Pt. II*, 164, 54–73, 2019.
- Hausfather, Z. and Peters, G. P.: Emissions – The “business as usual” story is misleading, *Nature*, 577, 618–620, 2020.
- Herrmann, M., Somot, S., Sevault, F., Estournel, C., and Déqué, M.: Modeling the deep convection in the northwestern Mediterranean Sea using an eddy-permitting and an eddy-resolving model: Case study of winter 1986–1987, *J. Geophys. Res.*, 113, C04011, <https://doi.org/10.1029/2006JC003991>, 2008.
- Herrmann, M., Diaz, F., Estournel, C., Marsaleix, P., and Ulses, C.: Impact of atmospheric and oceanic interannual variability on the North Western Mediterranean Sea pelagic planktonic ecosystem and associated carbon cycle, *J. Geophys. Res. Oceans*, 118, 5792–5813, <https://doi.org/10.1002/jgrc.20405>, 2013.
- Herrmann, M., Estournel, C., Adloff, F., and Diaz, F.: Impact of climate change on the northwestern Mediterranean Sea pelagic planktonic ecosystem and associated carbon cycle, *J. Geophys. Res.-Oceans*, 119, 5815–5836, <https://doi.org/10.1002/2014JC010016>, 2014.

- Ibrahim, O., Mohamed, B., and Nagy, H.: Spatial Variability and Trends of Marine Heat Waves in the Eastern Mediterranean Sea over 39 Years, *J. Mar. Sci. Eng.*, 9, 643, <https://doi.org/10.3390/jmse9060643>, 2021.
- IPCC AR5 Climate Change 2014: Synthesis Report. Contribution of Working Groups I, II and III to the Fifth Assessment Report of the Intergovernmental Panel on Climate Change, 2014.
- Keeling, R. F., Kortzinger, A., and Gruber, N.: Ocean Deoxygenation in a Warming World, *Ann. Rev. Mar. Sci.*, 2, 199–229, 2010.
- Kwiatkowski, L., Torres, O., Bopp, L., Aumont, O., Chamberlain, M., Christian, J. R., Dunne, J. P., Gehlen, M., Ilyina, T., John, J. G., Lenton, A., Li, H., Lovenduski, N. S., Orr, J. C., Palmieri, J., Santana-Falcón, Y., Schwinger, J., Séférian, R., Stock, C. A., Tagliabue, A., Takano, Y., Tjiputra, J., Toyama, K., Tsujino, H., Watanabe, M., Yamamoto, A., Yool, A., and Ziehn, T.: Twenty-first century ocean warming, acidification, deoxygenation, and upper-ocean nutrient and primary production decline from CMIP6 model projections, *Biogeosciences*, 17, 3439–3470, <https://doi.org/10.5194/bg-17-3439-2020>, 2020.
- Lamon, L., Rizzi, J., Bonaduce, A., Dubois, C., Lazzari, P., Ghenim, L., Gana, S., Somot, S., Li, L., Melaku Canu, D., Solidoro, C., Pinardi, N., and Marcomini, A.: An ensemble of models for identifying climate change scenarios in the Gulf of Gabes, Tunisia, *Reg. Environ. Change*, 14, 31–40, <https://doi.org/10.1007/s10113-013-0430-x>, 2014.
- Lavigne, H., D’Ortenzio, F., Ribera D’Alcalá, M., Claustre, H., Sauzède, R., and Gačić, M.: On the vertical distribution of the chlorophyll a concentration in the Mediterranean Sea: a basin-scale and seasonal approach, *Biogeosciences*, 12, 5021–5039, <https://doi.org/10.5194/bg-12-5021-2015>, 2015.
- Lascaratos, A.: Estimation of deep and intermediate water mass formation rates in the Mediterranean Sea, *Deep-Sea Res. Pt. II*, 40, 1327–1332, 1993.
- Lazzari, P., Solidoro, C., Ibello, V., Salon, S., Teruzzi, A., Béranger, K., Colella, S., and Crise, A.: Seasonal and inter-annual variability of plankton chlorophyll and primary production in the Mediterranean Sea: a modelling approach, *Biogeosciences*, 9, 217–233, <https://doi.org/10.5194/bg-9-217-2012>, 2012.
- Lazzari, P., Mattia, G., Solidoro, C., Salon, S., Crise, A., Zavatarelli, M., Oddo, P., and Vichi M.: The impacts of climate change and environmental management policies on the trophic regimes in the Mediterranean Sea: Scenario analyses, *J. Marine Syst.*, 135, 137–149, 2014.
- Lazzari, P., Solidoro, C., Salon, S., and Bolzon, G.: Spatial variability of phosphate and nitrate in the Mediterranean Sea: A modeling approach, *Deep-Sea Res.*, 108, 39–52, 2016.
- Lionello, P., Abrantes, F., Congedi, L., Dulac, F., Gačić, M., Gomis, D., Goodess, C., Hoff, H., Kutiel, H., Luterbacher, J., Planton, S., Reale, M., Schröder, K., Struglia, M. V., Toreti, A., Tsimplis, M., Ulbrich, U., and Xoplaki, E.: Introduction: Mediterranean Climate: Background Information, in: *The Climate of the Mediterranean Region. From the Past to the Future*, edited by: Lionello, P., Elsevier, Amsterdam, Netherlands, XXXV–IXXX, ISBN: 9780124160422, 2012.
- Lovato, T.: Mediterranean Sea marine physical simulations under CMIP5 historical and future scenario projections for the 21st century, CMCC DDS [data set], <https://dds.cmcc.it/#/dataset/medsea-cmip5-projections-physics>, last access: 21 July 2022.
- Lovato, T., Vichi, M., and Oddo, P.: High-resolution simulations of Mediterranean Sea physical oceanography under current and scenario climate conditions: model description, assessment and scenario analysis, CMCC Research Paper, 207, RP0207.2013, 2013.
- Macias, D. M., Garcia-Gorriz, E., and Stips, A.: Productivity changes in the Mediterranean Sea for the twenty-first century in response to changes in the regional atmospheric forcing, *Front. Mar. Sci.*, 2, 79, <https://doi.org/10.3389/fmars.2015.00079>, 2015.
- Macias, D., Stips, A., and Garcia-Gorriz, E.: The relevance of deep chlorophyll maximum in the open Mediterranean Sea evaluated through 3D hydrodynamic-biogeochemical coupled simulations, *Ecol. Model.*, 281, 26–37, 2014.
- Macias, D., Garcia-Gorriz, E., and Stips, A.: Deep winter convection and phytoplankton dynamics in the NW Mediterranean Sea under present climate and future (horizon 2030) scenarios, *Sci. Rep.*, 22, 1–15, <https://doi.org/10.1038/s41598-018-24965-0>, 2018.
- Madec, G.: NEMO Ocean Engine, Note du Pôle de modélisation, no. 27, Institut Pierre-Simon Laplace (IPSL), France, 2008.
- Mantziafou, A. and Lascaratos, A.: An eddy resolving numerical study of the general circulation and deep-water formation in the Adriatic Sea, *Deep-Sea Res. Pt. I*, 51, 251–292, 2004.
- Mantziafou, A. and Lascaratos, A.: Deep-water formation in the Adriatic Sea: Interannual simulations for the years 1979–1999, *Deep Sea Res. Pt. I*, 55, 1403–1427, 2008.
- Mathbout, S., Lopez-Bustins, J. A., Royé, D., and Martin-Vide, J.: Mediterranean-Scale Drought: Regional Datasets for Exceptional Meteorological Drought Events during 1975–2019, *Atmosphere*, 12, 941, <https://doi.org/10.3390/atmos12080941>, 2021.
- MedECC: Climate and Environmental Change in the Mediterranean Basin – Current Situation and Risks for the Future. First Mediterranean Assessment Report (Version 1), Zenodo, <https://doi.org/10.5281/zenodo.4768833>, 2020.
- Morel, A. and Gentili, B.: The dissolved yellow substance and the shades of blue in the Mediterranean Sea, *Biogeosciences*, 6, 2625–2636, <https://doi.org/10.5194/bg-6-2625-2009>, 2009.
- Moss, R. H., Edmonds, J. A., Hibbard, K. A., Manning, M. R., Rose, S. K., Van Vuuren, D. P., and Meehl, G. A.: The next generation of scenarios for climate change research and assessment, *Nature*, 463, 747–756, 2010.
- Moullec, F., Barrier, N., Drira, S., Guilhaumon, F., Marsaleix, P., Somot, S., Ulses, C., Velez, L., and Shin, Y. J.: An end-to-end model reveals losers and winners in a warming Mediterranean Sea, *Front. Mar. Sci.*, 6, 345, <https://doi.org/10.3389/fmars.2019.00345>, 2019.
- Moutin, T. and Raimbault, P.: Primary production, carbon export and nutrients availability in Western and Eastern Mediterranean Sea in early summer 1996 (MINOS cruise), *J. Marine Syst.*, 33/34, 273–288, 2002.
- Moutin, T. and Prieur, L.: Influence of anticyclonic eddies on the Biogeochemistry from the Oligotrophic to the Ultraoligotrophic Mediterranean (BOUM cruise), *Biogeosciences*, 9, 3827–3855, <https://doi.org/10.5194/bg-9-3827-2012>, 2012.
- Myers, P. G. and Haines, K.: Stability of the Mediterranean’s thermohaline circulation under modified surface evaporative fluxes, *J. Geophys. Res.*, 107, <https://doi.org/10.1029/2000JC000550>, 2002.

- Nittis, K. and Lascaratos, A.: Diagnostic and prognostic numerical studies of LIW formation, *J. Mar. Syst.*, 18, 179–195, 1998.
- O'Connor, M. I., Gilbert, B., and Brown, C. J.: Theoretical predictions for how temperature affects the dynamics of interacting herbivores and plants, *The American Naturalist*, 178, 626–638, 2011.
- Oddo, P., Adani, M., Pinardi, N., Fratianni, C., Tonani, M., and Pettenuzzo, D.: A nested Atlantic-Mediterranean Sea general circulation model for operational forecasting, *Ocean Sci.*, 5, 461–473, <https://doi.org/10.5194/os-5-461-2009>, 2009.
- O'Neill, B. C., Tebaldi, C., van Vuuren, D. P., Eyring, V., Friedlingstein, P., Hurtt, G., Knutti, R., Krieglner, E., Lamarque, J.-F., Lowe, J., Meehl, G. A., Moss, R., Riahi, K., and Sanderson, B. M.: The Scenario Model Intercomparison Project (ScenarioMIP) for CMIP6, *Geosci. Model Dev.*, 9, 3461–3482, <https://doi.org/10.5194/gmd-9-3461-2016>, 2016.
- Pagès, R., Baklouti, M., Barrier, N., Ayache, M., Sevault, F., Somot, S., and Moutin, T.: Projected Effects of Climate-Induced Changes in Hydrodynamics on the Biogeochemistry of the Mediterranean Sea Under the RCP 8.5 Regional Climate Scenario, *Front. Mar. Sci.*, 7, 957, <https://doi.org/10.3389/fmars.2020.563615>, 2020.
- Planton, S., Lionello, P., Artale, V., Aznar, R., Carrillo, A., Colin, J., Congedi, L., Dubois, C., Elizalde, A., Gualdi, S., Hertig, E., Jacobeit, J., Jordà, G., Li, L., Mariotti, A., Piani, C., Ruti, P., Sanchez-Gomez, E., Sannino, G., Sevault, F., Somot, S., and Tsimplis, M.: The Climate of the Mediterranean Region in Future Climate, in: *The Climate of the Mediterranean Region. From the Past to the Future*, edited by: Lionello, P., Elsevier, Amsterdam, Netherlands, Projections, 449–502, ISBN 978-0-12-416042-2, 2012.
- Powley, H. R., Krom, M. D., and Van Cappellen, P.: Circulation and oxygen cycling in the Mediterranean Sea: Sensitivity to future climate change, *J. Geophys. Res.-Oceans*, 121, 8230–8247, <https://doi.org/10.1002/2016JC012224>, 2016.
- Ramirez-Romero, E., Jordà, G., Amores, A., Kay, S., Segura-Noguera, M., Macias, D. M., Maynou, F., Sabatés, A., and Catalán, I. A.: Assessment of the Skill of Coupled Physical–Biogeochemical Models in the NW Mediterranean, *Front. Mar. Sci.*, 7, 497, <https://doi.org/10.3389/fmars.2020.00497>, 2020.
- Reale, M., Giorgi, F., Solidoro, C., Di Biagio, V., Di Sante, F., Mariotti, L., Farneti, R., and Sannino, G.: The Regional Earth System Model RegCM-ES: Evaluation of the Mediterranean climate and marine biogeochemistry, *J. Adv. Model. Earth Sy.*, 12, e2019MS001812, <https://doi.org/10.1029/2019MS001812>, 2020a.
- Reale, M., Salon, S., Somot, S., Solidoro, C., Giorgi, F., Cossarini, G., Lazzari, P., Crise, A., and Sevault, F.: Influence of large-scale atmospheric circulation patterns on nutrients dynamics in the Mediterranean Sea in the extended winter season (October–March) 1961–1999, *Clim. Res.*, 82, 117–136, <https://doi.org/10.3354/cr01620>, 2020b.
- Reale, M., Cossarini, G., Lazzari, P., Lovato, T., Bolzon, G., Masina, S., Solidoro, C., and Salon, S.: Mediterranean Sea marine biogeochemistry simulations under CMIP5 future scenario projections for the 21st century, CMCC DDS [data set], <https://dds.cmcc.it/#/dataset/medsea-cmip5-projections-biogeochemistry>, last access: 21 July 2022.
- Richon, C., Dutay, J.-C., Dulac, F., Wang, R., and Balkanski, Y.: Modeling the biogeochemical impact of atmospheric phosphate deposition from desert dust and combustion sources to the Mediterranean Sea, *Biogeosciences*, 15, 2499–2524, <https://doi.org/10.5194/bg-15-2499-2018>, 2018.
- Richon, C., Dutay, J.-C., Bopp, L., Le Vu, B., Orr, J. C., Somot, S., and Dulac, F.: Biogeochemical response of the Mediterranean Sea to the transient SRES-A2 climate change scenario, *Biogeosciences*, 16, 135–165, <https://doi.org/10.5194/bg-16-135-2019>, 2019.
- Salon, S., Cossarini, G., Bolzon, G., Feudale, L., Lazzari, P., Teruzzi, A., Solidoro, C., and Crise, A.: Novel metrics based on Biogeochemical Argo data to improve the model uncertainty evaluation of the CMEMS Mediterranean marine ecosystem forecasts, *Ocean Sci.*, 15, 997–1022, <https://doi.org/10.5194/os-15-997-2019>, 2019.
- Schroeder, K., Garcia-Lafuente, J., Josey, S. A., Artale, V., Nardelli, B. B., Carrillo, A., Gačić, M., Gasparini, G. P., Herrmann, M., Lionello, P., Ludwig, W., Millot, C., Özsoy, E., Pisacane, G., Sánchez-Garrido, J. C., Sannino, G., Santoleri, R., Somot, S., Struglia, M., Stanev, E., Taupier-Letage, I., Tsimplis, M. N., Vargas-Yáñez, M., Zervakis, V., and Zodiatis, G.: Circulation of the Mediterranean Sea and its Variability, in: *The Climate of the Mediterranean Region: From the Past to the Future*, edited by: Lionello, P., Elsevier Inc., 187–256, <https://doi.org/10.1016/B978-0-12-416042-2.00003-3>, 2012.
- Scoccimarro, E., Gualdi, S., Bellucci, A., Sanna, A., Fogli, P. G., Manzini, E., Vichi, M., Oddo, P., and Navarra, A.: Effects of Tropical Cyclones on Ocean Heat Transport in a High Resolution Coupled General Circulation Model, *J. Climate*, 24, 4368–4384, 2011.
- Shepherd, J. G., Brewer, P. G., Oschlies, A., and Watson, A. J.: Ocean ventilation and deoxygenation in a warming world: introduction and overview, *Philos. T. R. Soc. A*, 375, 20170240, <https://doi.org/10.1098/rsta.2017.0240>, 2017.
- Simoncelli, S., Fratianni, C., Pinardi, N., Grandi, A., Drudi, M., Oddo, P., and Dobricic, S.: Mediterranean Sea Physical Reanalysis (CMEMS MED-Physics), Copernicus Monitoring Environment Marine Service (CMEMS), [data set], <https://www.cmcc.it/mediterranean-sea-physical-reanalysis-cmems-med-physics> (last access: 31 October 2021), 2019.
- Siokou-Frangou, I., Christaki, U., Mazzocchi, M. G., Montresor, M., Ribera d'Alcalá, M., Vaqué, D., and Zingone, A.: Plankton in the open Mediterranean Sea: a review, *Biogeosciences*, 7, 1543–1586, <https://doi.org/10.5194/bg-7-1543-2010>, 2010.
- Sitz, L. E., Di Sante, F., Farneti, R., Fuentes-Franco, R., Coppola, E., Mariotti, L., Reale, M., Sannino, G., Barreiro, M., Nogherotto, R., Giuliani, G., Graffino, G., Solidoro, C., Cossarini, G., and Giorgi, F.: Description and evaluation of the Earth System Regional Climate Model (Reg CM-ES), *J. Adv. Model. Earth Sy.*, 9, 1863–1886, <https://doi.org/10.1002/2017MS000933>, 2017.
- Solidoro, C., Cossarini, G., Lazzari, P., Galli, G., Bolzon, G., Somot, S., Sevault, F., and Salon, S.: Modelling carbon budgets in the Mediterranean Sea ecosystem under contemporary and future climate, *Front. Mar. Sci.*, 8, <https://doi.org/10.3389/fmars.2021.781522>, 2022.
- Somot, S., Sevault, F., and Déqué, M.: Transient climate change scenario simulation of the Mediterranean Sea for the 21st century

- using a high-resolution ocean circulation model, *Clim. Dynam.*, 27, 851–879, <https://doi.org/10.1007/s00382-006-0167-z>, 2006.
- Somot, S., Houpert, L., Sevault, F., Testor, P., Bosse, A., Taupier-Letage, I., Bouin, M., Waldman, R., Cassou, C., Sanchez-Gomez, E., Durrieu de Madron, X., Adloff, F., Nabat, P., and Herrmann, M.: Characterizing, modelling and understanding the climate variability of the deep water formation in the North-Western Mediterranean Sea, *Clim. Dynam.*, 51, 1179–1210, <https://doi.org/10.1007/s00382-016-3295-0>, 2018.
- Soto-Navarro, J., Jordá, G., Amores, A., Cabos, W., Somot, S., Sevault, F., Macias, D., Djurdjevic V., Sannino G., Li, L., and Sein, D.: Evolution of Mediterranean Sea water properties under climate change scenarios in the Med-CORDEX ensemble, *Clim. Dyn.*, 54, 2135–2165, <https://doi.org/10.1007/s00382-019-05105-4>, 2020.
- Stöven, T. and Tanhua, T.: Ventilation of the Mediterranean Sea constrained by multiple transient tracer measurements, *Ocean Sci.*, 10, 439–457, <https://doi.org/10.5194/os-10-439-2014>, 2014.
- Taylor, K. E., Stouffer, R. J., and Meehl, G. A.: An Overview of CMIP5 and the Experiment Design, *B. Am. Meteorol. Soc.*, 93, 485–498, <https://doi.org/10.1175/BAMS-D-11-00094.1>, 2012.
- Teruzzi, A., Bolzon, G., Salon, S., Lazzari, P., Solidoro, C., and Cossarini, G.: Assimilation of coastal and open sea biogeochemical data to improve phytoplankton simulation in the Mediterranean Sea, *Ocean Model.*, 132, 46–60, 2018.
- Teruzzi, A., Bolzon, G., Cossarini, G., Lazzari, P., Salon, S., Crise, A., and Solidoro, C.: Mediterranean Sea Biogeochemical Reanalysis (CMEMS MED-Biogeochemistry), Copernicus Monitoring Environment Marine Service (CMEMS) [data set], <https://www.cmcc.it/doi/mediterranean-sea-biogeochemical-reanalysis-cmems-med-biogeochemistry> (last access: 31 January 2021), 2019.
- Teruzzi, A., Feudale, L., Bolzon, G., Lazzari, P., Salon, S., Di Biagio, V., Coidessa, G., and Cossarini, G.: Mediterranean Sea Biogeochemical Reanalysis (CMEMS MED-Biogeochemistry, MedBFM3 system) (Version 1) Copernicus Monitoring Environment Marine Service (CMEMS) [data set], https://doi.org/10.25423/CMCC/MEDSEA_MULTYEAR_BGC_006_008_MEDBFM3I, 2021.
- Van Apeldoorn, D. and Bouwman, L.: SES land-based runoff and nutrient load data (1980–2000), Deliverable 4.6, http://www.perseus-net.eu/assets/media/PDF/deliverables/3321.6_Final.pdf, (last access: 5 February 2020), 2014.
- Velaoras, D., Papadopoulos, V. P., Kontoyiannis, H., Cardin, V., and Civitarese, G.: Water masses and hydrography during April and June 2016 in the cretan sea and cretan passage (Eastern Mediterranean Sea), *Deep-Sea Res. Pt. II*, 164, 25–40, 2019.
- Vichi, M., Allen, J. I., Masina, S., and Hardman-Mountford, N. J.: The emergence of ocean biogeochemical provinces: A quantitative assessment and a diagnostic for model evaluation, *Global Biogeochem. Cy.*, 25, GB2005, <https://doi.org/10.1029/2010GB003867>, 2011.
- Vichi, M., Cossarini, G., Gutierrez Mlot, E., Lazzari, P., Lovato, T., Mattia, G., Masina, S., McKiver, W., Pinardi, N., Solidoro, C., and Zavatarelli, M.: The Biogeochemical Flux Model (BFM): Equation Description and User Manual. BFM version 5 (BFM-V5), Release 1.0, BFM Report series No. 1, March 2013, CMCC, Bologna, Italy, 87 pp., <http://bfm-community.eu> (last access: 30 October 2021), 2015.
- Waldman, R., Brüggemann, N., Bosse, A., Spall, M., Somot, S., and Sevault, F.: Overturning the Mediterranean thermohaline circulation, *Geophys. Res. Lett.*, 45, 8407–8415, <https://doi.org/10.1029/2018GL078502>, 2018.
- Wimart-Rousseau, C., Lajaunie-Salla, K., Marrec, P., Wagener, T., Raimbault, P., Lagadec, V., Lafont, M., Garcia, N., Diaz, F., Pinazo, C., Yohia, C., Garcia, F., Xueref-Remy, I., Blanc, P., Armengaud, A., and Lefèvre, D.: Temporal variability of the carbonate system and air-sea CO₂ exchanges in a Mediterranean human-impacted coastal site, *Estuar. Coast. Shelf S.*, 236, 106641, <https://doi.org/10.1016/j.ecss.2020.106641>, 2020.
- Wolf-Gladrow, D. A., Zeebe, R. E., Klaas, C., Körtzinger, A., and Dickson, A. G.: Total alkalinity, the explicit conservative expression and its application to biogeochemical processes, *Mar. Chem.*, 106, 287–300, 2007.
- Zunino, S., Canu, D. M., Bandelj, V., and Solidoro, C.: Effects of ocean acidification on benthic organisms in the Mediterranean Sea under realistic climatic scenarios: a meta-analysis, *Regional Studies in Marine Science*, 10, 86–96, 2017.
- Zunino, S., Canu, D. M., Zupo, V., and Solidoro, C.: Direct and indirect impacts of marine acidification on the ecosystem services provided by coralligenous reefs and seagrass systems, *Global Ecology and Conservation*, 18, e00625, <https://doi.org/10.1016/j.gecco.2019.e00625>, 2019.
- Zunino, S., Libralato, S., Melaku Canu, D., Prato G., and Solidoro C.: Impact of Ocean Acidification on Ecosystem Functioning and Services in Habitat-Forming Species and Marine Ecosystems, *Ecosystems*, 24, 1561–1575, <https://doi.org/10.1007/s10021-021-00601-3>, 2021.